RMIB GERB Processing - SEVIRI Processing : Spectral Modeling

Nicolas Clerbaux, Steven Dewitte

1st February 2002

MSG-RMIB-GE-TN-0005

Contents

CHANGE RECORD

Issue	Date	Approved by	Reason for change
Version 1	12/07/1999		new document
Version 1.1	29/09/99		CDR review

1 Introduction

1.1 Purpose of this document

The purpose of this document is to give an overview of the spectral modeling module within the 'SEVIRI Processing' subsystem of the near real time RMIB GERB Processing (RGP) system.

1.2 Scope of this document

This document does not describe the complete RGP nor the complete SEVIRI processing. The role of the SEVIRI Processing within the RGP is described in more detail in MSG-RMIB-GE-TN-0004. The other modules of the SEVIRI processing, the scene identification module and the angular modeling module, are described in MSG-RMIB-GE-TN-0007 and MSG-RMIB-GE-TN-0008 respectively.
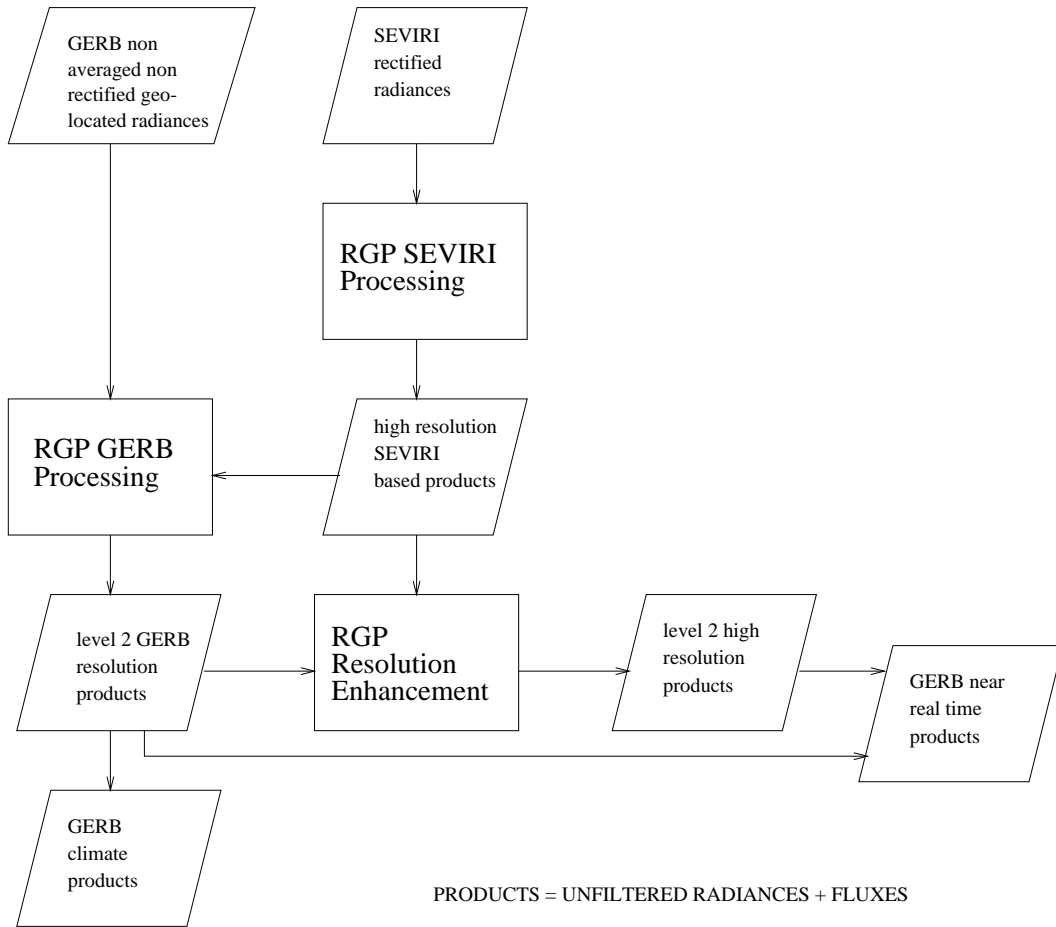
Figure 1: Division into subsystems of the RMIB GERB Processing. The three blocks 'RGS SEVIRI Processing', 'RGS GERB Processing' and 'RGS Resolution Enhancement' are executed in sequential order.

2 Role within the RGS

The RMIB part of the GERB ground segment consists in total of three subsystems: 'RMIB SEVIRI procesing', 'RMIB GERB processing' and 'Resolution enhancement', to be executed in sequential order. See also figure 1.

The subsystem 'RGS SEVIRI Processing' has as input full resolution SEVIRI spectrally narrow band radiances and as output SEVIRI pixel resolution filtered radiance estimates and broadband unfiltered estimates. Those outputs are referred to as 'high resolution SEVIRI based products'.

The subsystem 'RGS GERB Processing' has as input the GERB measured filtered broadband radiances as well as the high resolution SEVIRI based products, and as output GERB broadband unfiltered fluxes. Those outputs are referred to as 'level 2 GERB resolution fluxes'.

The subsystem 'Resolution enhancement' has as input the high resolution SEVIRI based flux estimates and the level 2 GERB resolution fluxes and as output high resolution fluxes that are compatible with the level 2 GERB resolution fluxes. Those outputs are referred to as 'level 2 high resolution fluxes'.

In the following sections a description of the spectral modelling part of the SEVIRI subsystem is given.

3 Generalities

3.1 Sources of radiances

Observing the Earth with a spectrometer, one can measure the radiance curve $L(\lambda)$. The measured radiance can be split in its two main sources : the solar reflected radiance $L_{sol}(\lambda)$ and the thermally emitted radiance $L_{th}(\lambda)$:

$$L(\lambda) \,=\, L_{sol}(\lambda) \,+\, L_{th}(\lambda)$$

Most of the applications of the satellite based broadband radiometer measurements (ERB, SRB, meteo, ...) need this splitting of the energy leaving the Earth into solar and thermal contributions. The final GERB level 2 products and derived products will be given for solar reflected and thermal radiation.

3.2 Broadband Radiometer Measurements

On the other hand, the broadband radiometer (e.g. GERB) measures also 2 radiances that do not match exactly the kind of emission. Using spectral filters, a broadband radiometer usually measures: the short wave radiance (approx $\lambda < 4\mu$) and the long wave radiance (approx $\lambda > 4\mu$) :

$$L_{sw} = \int_0^\infty L(\lambda)\,\varphi_{sw}(\lambda)\,d\lambda \,=\, \int_0^\infty (L_{sol}(\lambda)\,+\,L_{th}(\lambda))\,\varphi_{sw}(\lambda)\,d\lambda$$

$$L_{sw} \,=\, L_{sw,sol} \,+\, L_{sw,th}$$

and

$$L_{lw} = \int_0^\infty L(\lambda)\,\varphi_{lw}(\lambda)\,d\lambda \,=\, \int_0^\infty (L_{sol}(\lambda)\,+\,L_{th}(\lambda))\,\varphi_{lw}(\lambda)\,d\lambda$$

$$L_{lw} \,=\, L_{lw,sol} \,+\, L_{lw,th}$$

where $\varphi_{sw}(\lambda)$ and $\varphi_{lw}(\lambda)$ are the short wave and long wave spectral response curves of the broadband radiometer. Obviously, the quantities $L_{sw,th}$ (the thermal energy caught by the short wave filter) and $L_{lw,sol}$ (the solar reflected energy caught by the long wave filter) are expected to be small with respect to the $L_{sw,sol}$ and $L_{lw,th}$.

3.3 Radiometric quantities to be Estimated from the Imager

The table 1 enumerates the 6 radiometric quantities that have to be estimated for all the imager pixels at all imager time slots. In the RMIB GERB ground segment, the filtered quantities are needed as input to the 'GERB processing' subsystem (see [AD6]). The estimation of the 2 unfiltered radiances L_{th}^{uf} and L_{sol}^{uf} is studied respectively in sections 5 and 6 hereafter. The estimation of the 4 filtered quantities $L_{sw,sol}$, $L_{lw,th}$, $L_{lw,sol}$ and $L_{sw,th}$ is studied in section 7 of this document.

solar reflected unfiltered radiance	$L_{sol}^{uf} = \int_0^\infty L_{sol}(\lambda)\,d\lambda$
thermal emission unfiltered radiance	$L_{th}^{uf} = \int_0^\infty L_{th}(\lambda)\,d\lambda$
solar BB radiometer short wave radiance	$L_{sw,sol}^{filt} = \int_0^\infty L_{sol}(\lambda)\,\varphi_{sw}(\lambda)\,d\lambda$
thermal BB radiometer long wave radiance	$L_{lw,th}^{filt} = \int_0^\infty L_{th}(\lambda)\,\varphi_{lw}(\lambda)\,d\lambda$
solar BB radiometer long wave radiance	$L_{lw,sol}^{filt} = \int_0^\infty L_{sol}(\lambda)\,\varphi_{lw}(\lambda)\,d\lambda$
thermal BB radiometer short wave radiance	$L_{sw,th}^{filt} = \int_0^\infty L_{th}(\lambda)\,\varphi_{sw}(\lambda)\,d\lambda$

Table 1: Definition of the 6 radiances that are used in the GERB Ground Segment at RMIB and that have to be estimated from the imager (e.g. SEVIRI). $L_{sol}(\lambda)$ and $L_{th}(\lambda)$ are the solar reflected and thermally emitted spectral radiance of the scene. $\varphi_{sw}(\lambda)$ and $\varphi_{lw}(\lambda)$ are the short wave and long wave spectral responses of the broadband radiometer instrument (e.g. GERB).

3.4   Imager characteristics

3.4.1   Introduction

Two imaging systems may be used in the GERB Ground Segment: the imager on the Meteosat-7 satellite and the SEVIRI imager on the future MSG-1 satellite. The Meteosat-7 imager is operational since June 1998 and is planned to remain operational at least until SEVIRI is fully operational. This imager is important for the development of the GERB ground segment at RMIB because it is planned to be used during the SEVIRI commisioning phase.

3.4.2   Meteosat-7 imager

Like the others imagers of the Meteosat series, the imager on the Meteosat-7 satellite has 3 spectral channels:

- a visible band channel (radiance L_{vis}),

- a water-vapor channel (radiance L_{wv}),

- a window channel (radiance L_{ir}).

3.4.3   SEVIRI imager

The future MSG imager, SEVIRI, has 12 spectral channels designed for meteorological applications. The table 2 gives the expected characteristics of these channels. This information is available from the SEVIRI Science Plan [SSP].

The HRV (High Resolution Visible) channel has neither the same spatial resolution nor the same coverage of the Earth's disk than the others channels. For this reason the HRV radiances will not be used for spectral modeling.

The $IR3.9\mu$ channel lies at the cut-off between short wave and long wave radiation and is sensitive for both the solar reflected energy L_{sol} and the thermally emitted energy L_{th}. For this reason, this channel is not used for spectral modeling. In section §5.3.5, a short study is done about the spectral modeling improvement that can be obtained during night using the IR 3.9 channel.

These two channels removed, spectral modeling takes as input 3 NB channels in the short wave part of the spectrum and 7 spectral channels in the thermal part of the spectrum.

channel name	type	#filter	μ_i	σ_i	lower (1%)	upper (99%)
HRV	BB visible	0				
VIS 0.6	visible "green"	1	0.635 μ	0.025μ	0.56μ	0.71μ
VIS 0.8	visible "red"	2	0.81μ	0.030μ	0.74μ	0.88μ
IR 1.6	NIR water/ice	3	1.64μ	0.061μ	1.50μ	1.78μ
IR 3.9	window	4	3.92μ	0.191μ	3.48μ	4.36μ
IR 6.2	water vapor	5	6.25μ	0.301μ	5.35μ	7.15μ
IR 7.3	water vapor	6	7.35μ	0.217μ	6.85μ	7.85μ
IR8.7	window	7	8.70μ	0.174μ	8.30μ	9.10μ
IR9.7	O_3	8	9.66μ	0.122μ	9.38μ	9.94μ
IR 10.8	window	9	10.8μ	0.435μ	9.8μ	11.8μ
IR12	window	10	12.0μ	0.435μ	11.0μ	13.0μ
IR 13.4	CO_2	11	13.4μ	0.435μ	12.4μ	14.4μ

Table 2: The 12 SEVIRI channels. The table gives for each channel: EUMETSAT names, type of channel, channel index (internal at RMIB), mean and standard deviation when the spectral filters are modeled with a Gaussian shape, expected lower and upper limits

3.4.4 Noise Level and Calibration Errors

The imaging systems on weather satellites do not provide error free radiances L_{ch}. These radiances are subject to noise and errors of calibration. These errors should be take into account in the design of the spectral modeling and will affect the estimated filtered and unfiltered radiances of table 1.

In the following, the NB imager radiances are randomly modified with :

$$\widetilde{L_{nb}} = L_{nb}\left(1 + \eta \aleph(0,1)\right)$$

where η is the "noise" level (often expressed in percent) and $\aleph(0,1)$ is the Normal distribution with mean value 0 and standard deviation 1.

In this study, the noise level η on the NB radiances of the imaging system on a weather satellite is estimated as:

short wave channels ($\lambda < 4\mu$)	$\eta = 5\%$
long wave channels ($\lambda > 4\mu$)	$\eta = 2\%$

The higher value of η for short wave radiances is due to the absence of on-board calibration device (integrating sphere, ...).

3.5 Broadband Radiometer Characteristics

3.5.1 Introduction

As the GERB short wave and long wave spectral filters are not yet available in a reliable form, the CERES filters are used for the preparation of the RMIB GERB Ground Segment. The CERES filters are expected to be close to the GERB filters.
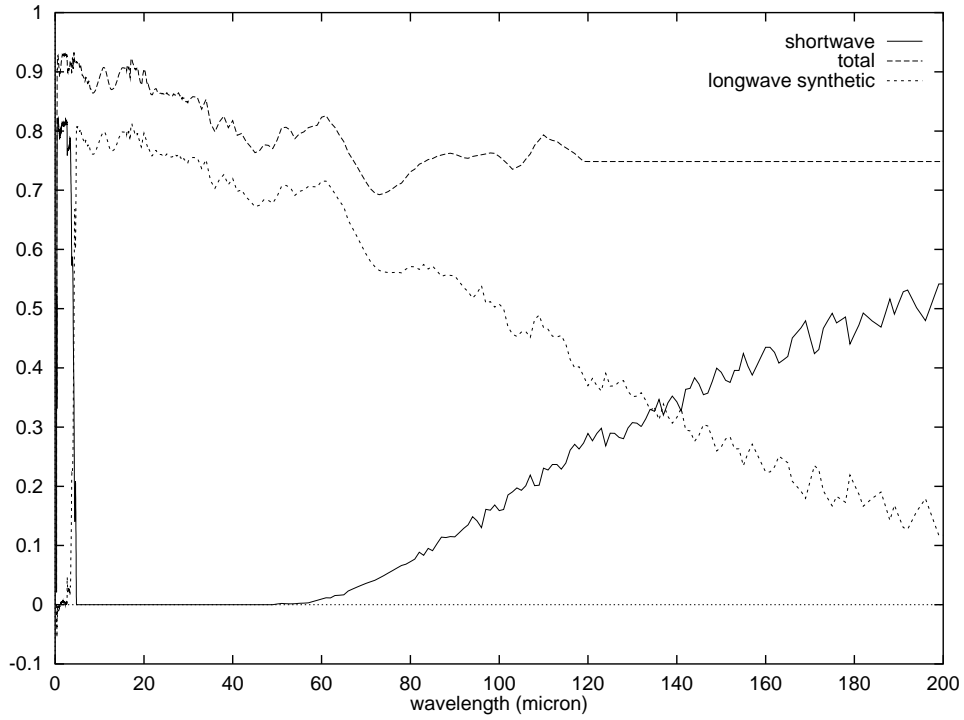
Figure 2: CERES short wave, total wave and synthetic long wave filters between 0 and 200 μ. For a detailed plotting in the range [0,10] μ, see figure 3.

3.5.2 Synthetic long wave filter

Basically the CERES and GERB instruments measure 2 radiances: the total wave radiance (without filter) and the short wave radiance (using a Quartz filter). From these two measures, a long wave synthetic radiance is defined by :

$$\phi_{lw}(\lambda) \,=\, \phi_{tot}(\lambda) \,-\, A\,\phi_{sw}(\lambda) \tag{1}$$

with the factor A taken in such a way that the synthetic long wave flux for a "solar spectrum scene" $F(\lambda)$ is null :

$$A \,=\, \frac{\int_0^\infty F(\lambda)\,\phi_{tot}(\lambda)\,d\lambda}{\int_0^\infty F(\lambda)\,\phi_{sw}(\lambda)\,d\lambda} \,=\, \frac{1176.4}{1043.9} \,=\, 1.127$$

3.5.3 Instrument Spectral Response Curves

The figures 2 and 3 show the shape of the short wave, total wave and synthetic long wave filters for the CERES broadband radiometer.
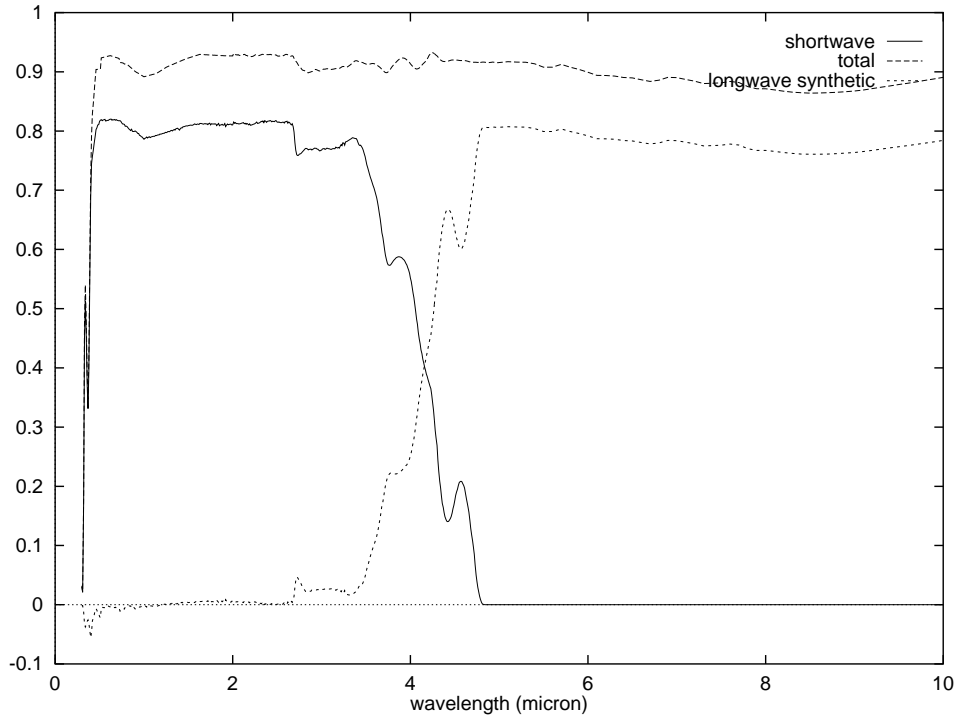
Figure 3: CERES short wave, total wave and synthetic long wave filters between 0 and 10μ.

4 Methodology

4.1 Implicit versus Explicit Scene Identification

The spectral modeling aims to characterize the repartition of the energy along the electro-magnetic spectrum and thus the kind of scene. Spectral modeling can then take as input an explicit scene identification information that means that the scene is known to belong to a class such as: ocean, snow, stratocumulus over land, ...

In the frame of the RMIB GERB spectral modeling, the spectral modeling is perform by implicit scene identification taking as inputs the NB radiances of an imaging device. In this case, a class should not be assigned to the scene but the results (in our case unfiltered or filtered broadband radiances) are dependent on the scene by regression on the input radiances.

4.2 Data Set of Scene Spectral Signatures

The design and tuning of the spectral modeling process is done using synthetic spectral signature curves L_{th} and L_{sol} of the Earth surface. These curves are built by radiative transfer computing under various Earth-atmosphere conditions. the radiative transfer code used at RMIB is SBDART (Santa Barbara Discrete ordinate Atmospheric Radiative Transfer, [SBDART]).

The building of these curves (input parameters used for the Earth-atmosphere system, ...) is described in an internal RMIB document [NC01].

For each scene (a given parametrisation of the Earth-atmosphere system), the following curves are built :

- L_{th,θ_v} : the spectral curve of the thermally emitted radiance at the TOA for the 9 different
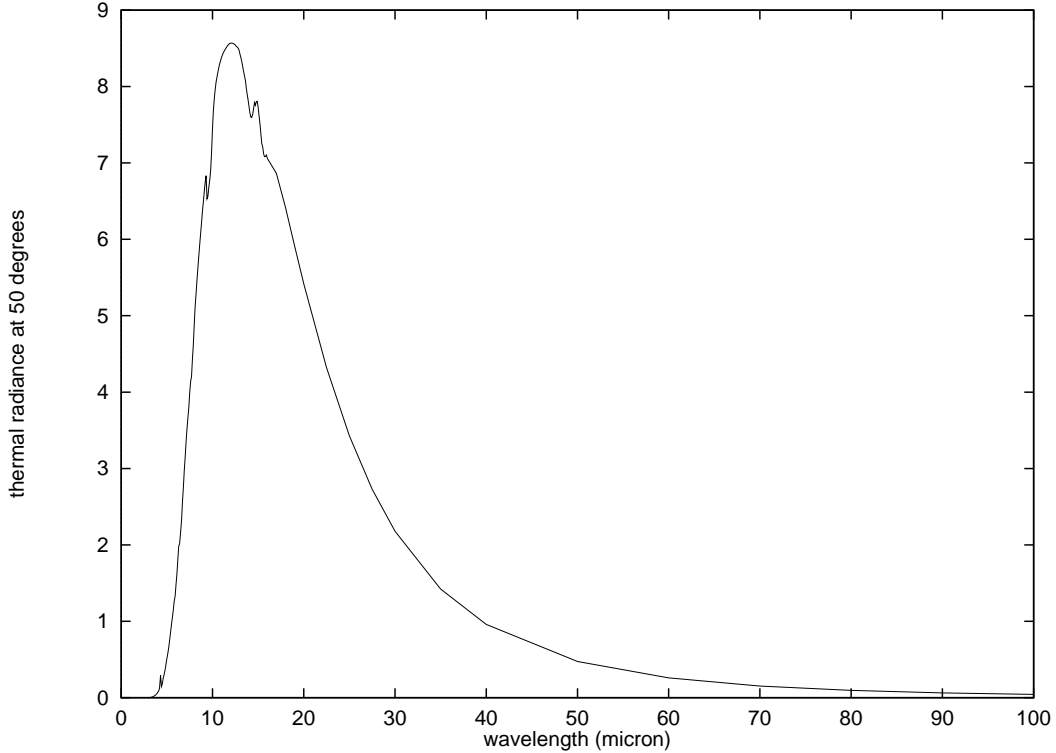
Figure 4: example of thermally emitted spectral radiance curve at the TOA, generated using SBDART for a viewing zenith angle of 50 degrees.

viewing zenith angles θ_v out of the set :

$$\theta_v = \{0^o, 10^o, 20^o, 30^o, 40^o, 50^o, 60^o, 70^o, 80^o\} \tag{2}$$

- L_{th,cs,θ_v} : idem as L_{th,θ_v} but without cloud layer (clear sky conditions)

- $F_{sol}(\lambda)$: the spectral curve of the reflected solar flux at the TOA

- $F_{sol,cs}(\lambda)$: idem as $F_{sol}(\lambda)$ but without cloud layer (clear sky conditions)

For the reflected solar energy, the flux is computed instead of the radiance because the radiative transfer code does not take into account bidirectional effect for the reflection on the Earth surface.

Illustration of these curves are given in figures 4 (thermal) and 5 (solar reflected).

The RMIB data set contains 2000 spectral curves that correspond to 2000 different Earth-atmosphere realizations. This data set is usually split in two equal parts : 1000 curves serve for spectral modeling tuning (least square parametrization) and the remaining 1000 curves serve for validation. This approach allows to detect and avoid the data overfitting problem.

4.3   Radiances Data Set Building

NB imager radiances (L_{ch}), BB radiometer radiances (L_{sw}^{filt} and L_{lw}^{filt}) and unfiltered radiances (L_{sol}^{uf} and L_{th}^{uf}) are computed by spectral integration of the spectral curves $L(\lambda) = L_{sol}(\lambda) + L_{th}(\lambda)$ with a spectral response curve $\phi(\lambda)$:
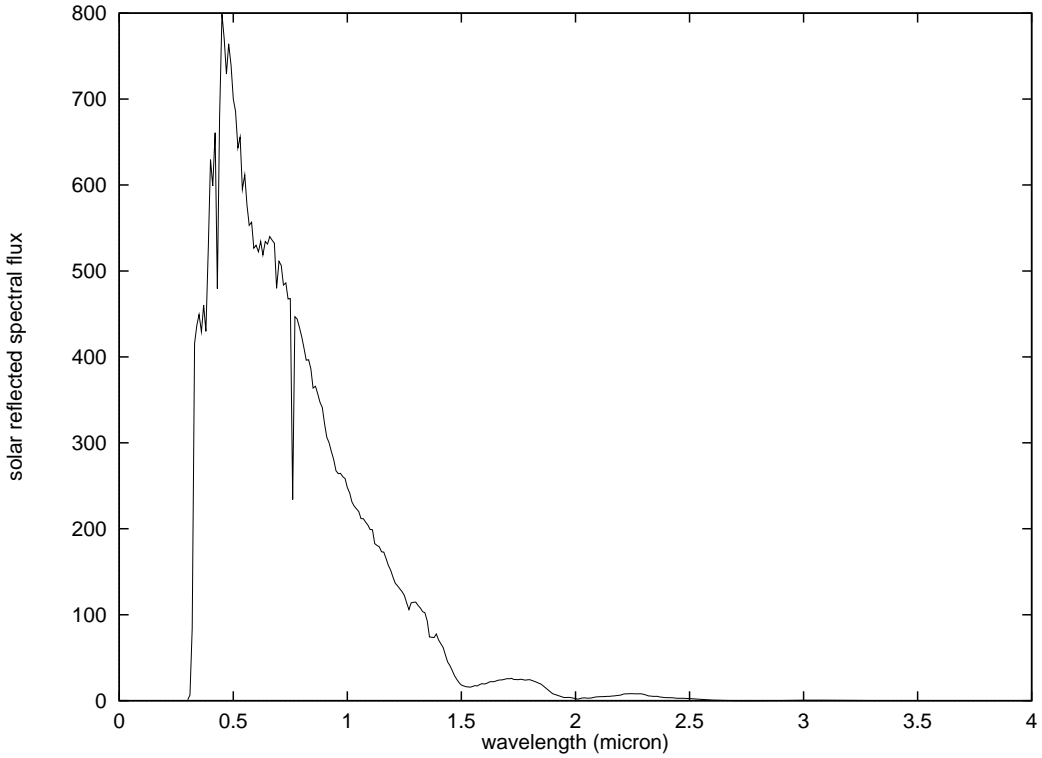
Figure 5: example of reflected solar spectral flux curve at the TOA, generated using SBDART.

$$L_i \;=\; \int_0^\infty L(\lambda)\,\phi_i(\lambda)\,d\lambda \tag{3}$$

The integration (3) is performed using the RMIB program "integral" (see [PINT]). The unfiltered radiances are computed using a flat filter $\phi(\lambda)$ between 0 and the ∞.

$$L^{uf} \;=\; \int_0^\infty L(\lambda)\,d\lambda \tag{4}$$

4.4   Least Mean Square

The radiances (unfiltered or filtered) to be estimated y are fitted with a polynomial regression on the NB radiances $\{L_{nb}\}$ of the imaging device :

$$\widetilde{y} = c_0 + c_1 L_1 + c_2 L_2 + ... + c_x L_n + . \, c_x L_1^2 + c_x L_1 L_2 + c_x L_2^2 + ... + c_x L_n^2 + ... \tag{5}$$

The best set of regression coefficients $\{c_i\}$ is supposed to be the one minimizing the residual mean square error on the estimated quantity y for the set of spectral curves. The residual error ϵ:

$$\epsilon = \sqrt{\frac{1}{N} \sum_{i=0}^{N} (\widetilde{y_i} \, - \, y_i)^2}$$

is often converted into relative residual error ϵ_r (in percent):

$$\epsilon_r = \frac{\epsilon}{\langle y \rangle}$$

$$\langle y \rangle = \frac{1}{N} \sum_{i=0}^{N} y_i$$

where the summation is done on the validation set of $N = 1000$ spectral curves.

4.5 Discarding of Variables

For a least square estimator, discarding of variables consists to set artificially some of the regression coefficients c_i at 0. For a similar residual error, the discarding of variables technique allows:

- (i) to increase the robustness of the estimator with respect to the input noise (specially for high order inputs),

- (ii) to overcome overfitting of the data (specially for restricted data sets) and

- (iii) additionally to save computation time.

Description and examples of discarding of variables techniques can be found in [MA79],§6.7 or [PLMS]. The program used at RMIB (*leastsq*) searches, for an increasing number of non-null coefficients, the coefficients configuration minimizing the residual error ϵ_r. The figure6 is a typical example of the decrease of ϵ_r when increasing number of non-null coefficients are used in a regression. On this curve, one can see that only three non-null coefficients are sufficient to fit the data. Using more coefficients than 3 coefficients complicates the interpretation of the resulting regression and can be dangerous when the input data are "noisy".
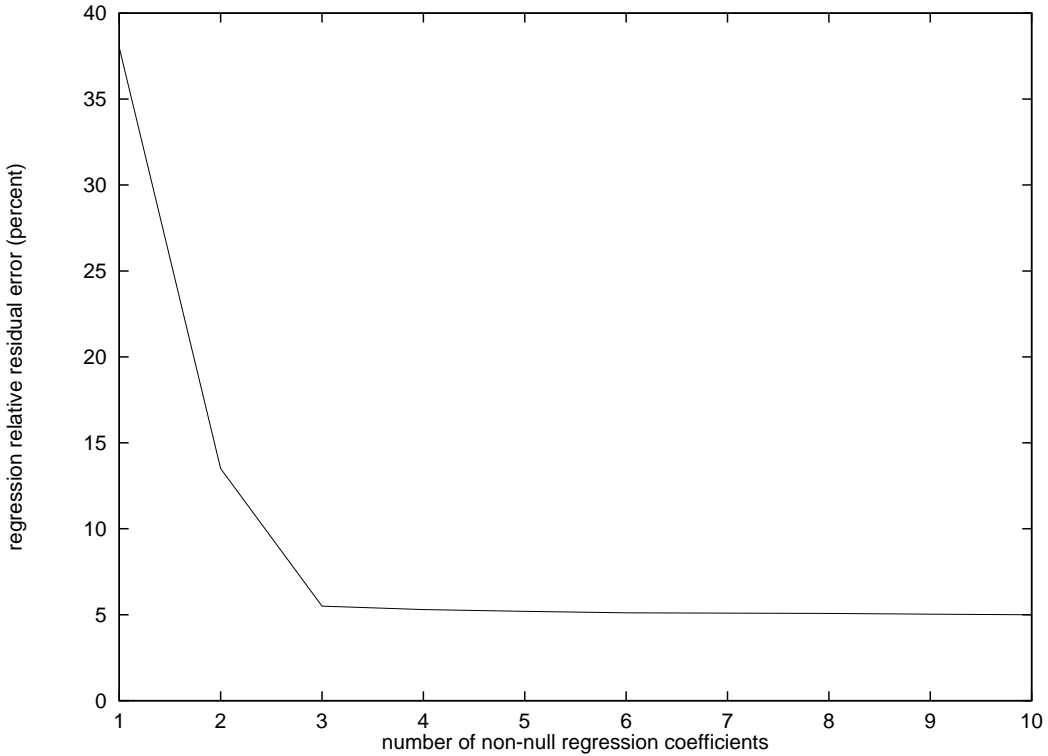
Figure 6: Typical shape of the least square residual error versus the number of non-null coefficients.

5 Estimate Thermal Unfiltered Radiance L_{th}^{uf} Using Imager Data

5.1 Problem statement

Here, the problem consists to find the function

$$L_{th}^{uf} = L_{th}^{uf}(\{L_{ch}\}) \tag{6}$$

that gives the best estimate of the unfiltered thermal radiance L_{th}^{uf} from the set of NB $\{L_{ch}\}$ of the imaging system. This best function is the one that minimizes the residual error ϵ on a set of spectral curves representative of the Earth's thermal emission. The estimate 6 is done using only the imager channels that are sensitive to thermally emitted radiation.

In the following, a typical viewing zenith angle θ_v of 50 degrees is used. The impact of viewing zenith angle on the estimation 6 is analyzed in section §5.5. The imager radiances are supposed to be contaminated with a noise level of $\eta = 2\%$ (see §3.4.4). The impact of the noise level η on the regression law and coefficients is studied in section §5.4.

5.2 Meteosat-7 case

5.2.1 Problem statement

This imager measures 2 radiances in the thermal part of the spectrum : the water-vapor radiance L_{wv} and the window radiance L_{ir} (see §3.4.2). With this imager, the problem becomes to find the function :

#coef	best law	ϵ_r (%)
1	$L_{th}^{uf} = 7.24\,L_{ir}$	18.33%
2	$L_{th}^{uf} = 27.8 + 4.46\,L_{ir}$	5.96%
3	$L_{th}^{uf} = 21.56 + 19.24\,L_{wv} + 3.45\,L_{ir}$	1.76%
4	$L_{th}^{uf} = 19.29 + 25.81\,L_{wv} + 3.49\,L_{ir} - 4.29\,L_{wv}^2$	1.68%
5		
6	...	
7		
8		
9		
10	all coefficients up to third order	1.56%

Table 3: Best laws for unfiltered thermal radiance L_{th}^{uf} estimation when an increasing number of regression coefficients are used (discarding of variables technique). The inputs are the 2 NB thermal radiances L_{wv} and L_{ir} of the Meteosat-7 imager. Viewing zenith angle is $\theta_v = 50^o$ and imager radiance noise level is $\eta = 2\%$.

$$L_{th}^{uf} = L_{th}^{uf}(L_{wv}, L_{ir})$$

Using a polynomial expansion up to the third order on the input radiances, one gets :

$$L_{th}^{uf} = c_0 + c_1 L_{wv} + c_2 L_{ir} + c_3 L_{wv}^2 + c_4 L_{wv} L_{ir} + c_5 L_{ir}^2 + \tag{7}$$

$$c_6 L_{wv}^3 + c_7 L_{wv}^2 L_{ir} + c_8 L_{wv} L_{ir}^2 + c_9 L_{ir}^3 \tag{8}$$

5.2.2 Results

The discarding of variables applied to the regression 8 gives the results summarized in table 3.

5.2.3 Discussion

Even using all coefficients up to the third order the overfitting phenomena seems not appear here. Nevertheless, high order terms do not provide noticeable improvement in the unfiltered radiance estimation. For simplicity and robustness, the 3 coefficients law should be chosen :

$$L_{th} = 21.56 + 19.24\,L_{wv} + 3.45\,L_{ir} \tag{9}$$

The relative residual error of the thermal unfiltered radiance inference is typically below $\epsilon_r < 2\%$, under the noise level on the input radiances which is $\eta = 2\%$ (effect of averaging).

5.3 The SEVIRI case

5.3.1 Problem statement

This imager measures 7 radiances in the thermal part of the spectrum (see §3.4.3)[1]. With this imager, the problem becomes to find the function :

$$L_{th}^{uf} = L_{th}^{uf}(L_{6.2\mu}, L_{7.3\mu}, L_{8.7\mu}, L_{9.7\mu}, L_{10.8\mu}, L_{12\mu}, L_{13.4\mu})$$

---

[1]During the day, the IR 3.8 channel is contaminated by reflected solar radiation. For this reason, this channel is not used to estimate unfiltered radiance from NB radiances. In section $5.3.5 hereafter, a study is done about the improvement that can be obtained during night using the IR 3.8 channel.

#coef	best law	ϵ_r (%)
1	$L_{th} = 17.81\, L_{13.4\mu}$	3.75%
2	$L_{th} = -5.79\, L_{7.3\mu} + 19.46\, L_{13.4\mu}$	3.53%
3	$L_{th} = 20.9 + 20.08\, L_{6.2\mu} + 6.06\, L_{12\mu}$	1.72%
4	$L_{th} = 15.06 + 11.77\, L_{6.2\mu} + 3.24\, L_{10.8\mu} + 6.93\, L_{13.4\mu}$	1.17%
5	$L_{th} = 16.27 + 12.64\, L_{6.2\mu} + 3.95\, L_{8.7\mu} + 2.15\, L_{12\mu} + 6.13\, L_{13.4\mu}$	1.10%
	...	
8	all coefficients up to the first order...	1.04%
	...	
36	all coefficients up to the second order...	0.82%
	...	
85	all coefficients up to the third order......	0.87%
	...	

Table 4: Best laws for unfiltered thermal radiance L_{th}^{uf} estimation when an increasing number of regression coefficients are used (discarding of variables technique). The inputs are the 7 NB thermal radiances of SEVIRI. Viewing zenith angle is $\theta_v = 50^o$ and imager radiance noise level is $\eta = 2\%$.

Using a polynomial expansion up to the second order on the input radiances, one gets :

$$L_{th}^{uf} = \alpha + \sum_{c=1}^{7} \beta_c\, L_c + \sum_{c=1}^{7} \sum_{c'=1}^{c} \gamma_{c,c'}\, L_c\, L_{c'} \tag{10}$$

5.3.2 Results

The discarding of variables applied to the regression 10 gives the results summarized in table 4.

5.3.3 Discussion

A (week) overfitting phenomena appears between the second and third order regression. High order terms do not provide noticeable improvement in the unfiltered radiance estimation. For simplicity and robustness, the 5 coefficients law can be chosen :

$$L_{th}^{uf} = 16.27 + 12.64\, L_{6.2\mu} + 3.95\, L_{8.7\mu} + 2.15\, L_{12\mu} + 6.13\, L_{13.4\mu}$$

The relative residual error of the thermal unfiltered radiance inference is typically close to $\epsilon_r \approx 1\%$, under the noise level on the input radiances which is $\eta = 2\%$ (effect of averaging).

For the sake of generality and simplicity, the regression using all radiances up to the first order is often used in the following:

$$L_{th}^{uf} = \beta_0 + \beta_1\, L_{6.2\mu} + \beta_2\, L_{7.3\mu} + \beta_3\, L_{8.7\mu} - \beta_4\, L_{9.7\mu} + \beta_5\, L_{10.8\mu} + \beta_6\, L_{12\mu} + \beta_7\, L_{13.4\mu} \tag{11}$$

in this case the best regression is :

$$L_{th}^{uf} = 17.4 + 10.69\, L_{6.2\mu} + 3.05\, L_{7.3\mu} + 3.03\, L_{8.7\mu} - 0.53\, L_{9.7\mu} + 1.22\, L_{10.8\mu} + 1.20\, L_{12\mu} + 5.51\, L_{13.4\mu} \tag{12}$$

used channels	ϵ_r (%)
all radiances	1.04
all exc. $L_{6.2\mu}$	1.40
all exc. $L_{7.3\mu}$	1.07
all exc. $L_{8.7\mu}$	1.08
all exc. $L_{9.7\mu}$	1.04
all exc. $L_{10.8\mu}$	1.08
all exc. $L_{12\mu}$	1.06
all exc. $L_{13.4\mu}$	1.42

Table 5: Consequences of the loss of one SEVIRI channel on the accuracy of the L_{th}^{uf} inference process. Viewing zenith angle is $\theta_v = 50^o$ and imager radiance noise level is $\eta = 2\%$.

5.3.4 Loss of channel(s)

Here, a short analysis is given on the consequences that the loss of one or multiple SEVIRI channel(s) could have on the spectral modeling. For this, we use the first order regression 11.

Table 5 shows the influence on the residual error ϵ_r if one SEVIRI channel is not available. Two of the 7 thermal SEVIRI channels appear to be "critical" for the estimation of the unfiltered thermal radiance L_{th}^{uf}: the CO_2 channel at 13.6μ and the first water vapor channel at 6.2μ. The loss of one of these channel increases the error with about 30 %! On the other hand, the loss of one of the others channel may not have great influence. If, simultaneously, the 13.6μ and 6.2μ are not available, the error increases dramatically up to 1.77% which is worse than using the 2 channels of the current Meteosat-7 !

input	ϵ_r (%)
all exc. . $L_{6.2\mu}$.and $L_{13.4\mu}$	1.77 %

5.3.5 Using the IR 3.9 channel during night

In this section, the improvement that could be obtained during night using the 3.9μ channel is estimated. As for the "loss of channel" study, the first order regression 11 will serve as reference for comparison.

input	relative error (%)
all thermal channels	1.04 %
all thermal channels + $L_{3.9\mu}$	1.02 %

The improvement should be considered as "insignificant" and the $IR\,3.9\mu$ channel will not be used in the spectral modeling part of the GERB ground segment at RMIB.

5.4 Imager noise influence

5.4.1 Statement

The results given before for the imager of Meteosat-7 and for SEVIRI were obtained using a typical $\eta = 2\%$ sensor noise (see §3.4.4). Here, the influence of the imager noise η on the unfiltered radiance estimation error ϵ_r is investigated.

η	ϵ_r	β_0	$\beta_{6.2\mu}$	$\beta_{7.3\mu}$	$\beta_{8.7\mu}$	$\beta_{9.7\mu}$	$\beta_{10.8\mu}$	$\beta_{12\mu}$	$\beta_{13.4\mu}$
0.00	0.61 %	13.861	8.970	0.651	3.429	-2.745	2.993	-1.942	9.705
0.01	0.79 %	15.338	10.096	1.261	3.570	-1.629	1.632	0.013	7.775
0.02	1.04 %	17.405	10.692	3.051	3.035	-0.539	1.218	1.200	5.514
0.03	1.27 %	18.974	10.680	4.737	2.898	0.101	1.179	1.549	4.085
0.05	1.72 %	20.764	10.430	6.682	3.128	0.952	1.161	1.636	2.663
0.10	2.86 %	22.279	10.126	7.715	3.504	2.552	1.122	1.516	1.622
0.20	5.19 %	23.756	9.489	7.268	3.667	3.982	1.096	1.388	1.194

Table 6: The relative residual error ϵ_r (%) and the first order regression coefficients $\{\beta_i\}$ of the first order regression 11 for increasing noise level η on the SEVIRI radiances.

5.4.2   Residual Error ϵ_r Versus Imager Noise η

The table 6 gives, for various noise level η of the SEVIRI imager, the best coefficients $\{\beta_i\}$ for the first order regression and the regression residual error ϵ_r. One can see that the relative residual error ϵ_r increases linearly with the imager noise level η:

$$\epsilon_r \approx 0.61\,\% + \eta\,23\%$$

At high noise level, the regression becomes like an "averaging" on the SEVIRI radiances[2]. At small noise level, the regression becomes "more intelligent" and takes advantage of the correlations: this explains the negative value for $\beta_{9.7\mu}$ and $\beta_{12\mu}$.

5.4.3   On the Importance of Carefully Estimate the Input Noise η

Imager noise η must be estimated carefully and should include both noise and calibration error. Ideally, this estimation should be done channel by channel. If the noise level is underestimated (for example when it is not taken into account), the regression becomes too "intelligent" and the performances may collapse. For example, the first order regression with a null noise level ($\eta = 0$) leads to the regression coefficients given in table 6 and an attractive residual error of $\epsilon_r = 0.61\%$. Using this regression but with input radiances subject to a noise level of $\eta = 5\%$ leads to an error of $\epsilon_r = 3.11\%$ which is nearly twice the error obtained if the correct noise level is taken into account ($\epsilon_r = 1.72\%$, see table 6)!

5.5   Angular dependency

5.5.1   Statement

The results given before for the imager of Meteosat-7 and for SEVIRI are obtained for a typical viewing zenith angle of $\theta_v = 50^o$. In this section, the dependency of the regression coefficients and residual error with the viewing zenith angle θ_v is studied.

5.5.2   Law and Error Versus Viewing Zenith Angle θ_v for Meteosat-7

Here, the best first order regression on the Meteosat-7 NB radiances and the associated residual errors ϵ_r are computed for the set (2) of viewing zenith angles θ_v:

$$L_{th}^{uf} = \beta_0(\theta_v) + \beta_1(\theta_v)\,L_{wv} + \beta_2(\theta_v)\,L_{ir} \tag{13}$$

θ_v	β_0	β_1	β_2	ϵ_r (%)
0°	21.654	17.617	3.613	1.7538
10°	21.658	17.662	3.608	1.7533
20°	21.647	17.837	3.589	1.7538
30°	21.637	18.121	3.558	1.7544
40°	21.614	18.568	3.512	1.7591
50°	21.564	19.240	3.447	1.7672
60°	21.462	20.266	3.358	1.7852
70°	21.227	21.922	3.235	1.8134
80°	20.632	24.947	3.074	1.8615

Table 7: Coefficients β_i and residual error ϵ_r of the first order regression 13 to estimate L_{th}^{uf} from the Meteosat-7 thermal radiances L_{wv} and L_{ir}. The noise level on the input radiance is $\eta = 2\%$.

θ_v	ϵ_r (%)	β_0	$\beta_{6.2\mu}$	$\beta_{7.3\mu}$	$\beta_{8.7\mu}$	$\beta_{9.7\mu}$	$\beta_{10.8\mu}$	$\beta_{12\mu}$	$\beta_{13.4\mu}$
0°	1.0525	18.06	10.03	3.10	2.93	-0.66	1.31	1.27	5.22
10°	1.0526	18.04	10.04	3.09	2.94	-0.65	1.31	1.27	5.24
20°	1.0533	17.97	10.16	3.05	2.96	-0.65	1.30	1.26	5.27
30°	1.0507	17.85	10.29	3.02	3.00	-0.63	1.28	1.23	5.33
40°	1.0471	17.67	10.48	2.99	3.03	-0.59	1.25	1.21	5.41
50°	1.0392	17.40	10.69	3.05	3.03	-0.53	1.21	1.20	5.51
60°	1.0246	17.03	10.84	3.31	2.97	-0.45	1.17	1.21	5.61
70°	0.9988	16.52	10.71	4.17	2.73	-0.30	1.14	1.32	5.62
80°	0.9920	15.80	9.19	7.21	2.00	-0.01	1.18	1.61	5.33

Table 8: Coefficients β_i and residual error ϵ_r of the first order regression11 to estimate L_{th}^{uf} from the SEVIRI thermal radiances. The relative residual error ϵ_r on the inferred unfiltered radiance L_{th}^{uf} is relatively independent on the viewing zenith angle θ_v. The noise level on the input radiance is $\eta = 2\%$.

One can see in table 7 that the residual error ϵ_r of the regression is relatively constant with the viewing zenith angle θ_v. The regression coefficients $\{\beta_i\}$ vary slowly with θ_v.When the viewing zenith angle θ_v increases, the weighting of the water vapor channel (β_1) increases and the weighting (β_2) of the window channel decreases. At grazing angles, the radiance is mainly due to thermal emission by upper-troposphere layers, this is the well-known limb darkening effect.

5.5.3 Law and error versus viewing angle for SEVIRI

Here, the first order regression 11 on SEVIRI radiances and the residual errors ϵ_r associated with these regressions are computed for the set (2) of viewing zenith angles θ_v. Results are summarized in table 8. One can see on table 8 that the residual error ϵ_r is relatively constant with the viewing zenith angle. The estimation of L_{th}^{uf} from NB radiances seems be a bit more accurate at grazing angle (residual error $\epsilon_r \cong 0.99\%$) than at nadir ($\epsilon_r \cong 1.05\%$). The regression coefficients $\{\beta_i\}$ show a smooth variation with θ_v.

5.5.4 Must the regression law be angular dependent ?

In the last section, a smooth variation of the regression coefficients with viewing zenith angle θ_v has been detected. Here, the question is : "may a same set of regression coefficients be used for

---

[2]the higher coefficients for the water vapor channels can be explained by the smaller radiances in these channel.

θ_v	$\epsilon_r\ (\%)$
0°	1.2826
10°	1.2693
20°	1.2320
30°	1.1708
40°	1.0982
50°	1.0392
60°	1.0629
70°	1.3096
80°	2.0817

Table 9: Relative residual error ϵ_r for the SEVIRI regression 11 with respect to the viewing zenith angle θ_v when the regression coefficients at $\theta_v = 50^o$ are used. The residual error ϵ_r increases dramatically at nadir and at grazing angle. a great dependency on the satellite viewing angle θ_v. Obviously, the error is minimal at 50°.

all the viewing zenith angles?".

Using the law at $\theta_v = 50^o$:

$$\beta_i = \{17.40, 10.69, 3.05, 3.03, -0.53, 1.21, 1.20, 5.51\}$$

the error of this law is computed for others viewing zenith angles. Results are summarized in table 9. Comparison of table 8 (where coefficients depend on θ_v) and table 9 (where coefficients do not depend on θ_v) shows that to be valid on a wide range of viewing zenith angles (from nadir to grazing angles), the regression coefficients β_i should be angular dependent:

$$\beta_i = \beta_i(\theta_v)$$

5.5.5 Discussion

The regression law to estimate L_{th}^{uf} from the imager NB radiances $\{L_c\}$ should clearly be dependent on the viewing zenith angle θ_v. In this case the residual error is relatively independent on θ_v. Without taking into account the angular dependency, the residual error increases of about 20% at nadir and 100% at 80°. For this reason, an angular dependent regression is adopted for the GERB Ground Segment at RMIB.

5.6 Conclusions and discussions

On this section, we have seen that :

1. The inference of the unfiltered thermal radiance L_{th}^{uf} from the NB radiances provided by an imaging device on weather satellites is possible.

2. The error of this inference decreases when the number of image thermal channel increases. This improvement is due to: (i) a better spectral modeling of the scene and (ii) an averaging of the noise level and calibration error that affect the imager radiances. This residual error can be estimated as: $\epsilon_r = 1.8\%$ for the imager of Meteosat-7 and $\epsilon_r = 1.0\%$ for SEVIRI.

3. A first order regression on the imager NB radiances is sufficient to estimate accurately and robustly L_{th}^{uf}. This was demonstrated for the imager on-board Meteosat-7 (2 thermal channels) and for SEVIRI (7 thermal channels). The use of higher order terms in the regression seems not be judicious: the regression will (over)fit the internal laws of the radiative transfer model which are simplifications of the real natural physics.

4. The level of accuracy η on the imager NB radiances measurements must be estimated carefully and should never be underestimated. The sources of inaccuracy on these radiances are due to sensor noise and error of calibration. A rough estimate for SEVIRI can be found in the SEVIRI Science Plan [SSP], chapters 3 and 5. From this, a Gaussian noise with $\eta = 2\%$ standard deviations was adopted for the input radiances.

5. The regression law must take into account the angular dependency on the viewing zenith angle θ_v. This dependence is due to a spectral dependency of the limb darkening function: at grazing angles the atmospheric windows disappear due to the great optical path through the atmosphere. In practice, the regression coefficients are computed for $\theta_v = \{0^o, 10^o, 20^o, 30^o, 40^o, 50^o, 60^o, 70^o, 80^o\}$.

6   Estimate Solar Reflected Unfiltered Radiance Using Imager Data

6.1   Introduction

6.1.1   Problem statement

Here, the problem consists to find the function

$$L_{sol}^{uf} = L_{sol}^{uf}(\{L_{ch}\}) \tag{14}$$

that gives the best estimate of the unfiltered solar reflected radiance L_{sol}^{uf} from the set of the NB radiances $\{L_{ch}\}$ of the imaging system. This best function is the one that minimizes residual error ϵ on a set of spectral curves representative of the Earth's solar reflection. The estimate 14 is done using only the imager channels that are sensible to solar reflected radiation and not to thermal radiation (the SEVIRI $IR3.8\mu$ channel is then rejected here).

The imager radiances are supposed to be contaminated with a noise level of $\eta = 5\%$ (see 3.4.4). The impact of noise level η on the regression law and coefficients is studied latter for the Meteosat-7 imager and for SEVIRI.

6.1.2   Radiative Model Limitation due to Lambertian Surfaces

The radiative transfer model used at RMIB (see [SBDART]) to build the data set of Earth's spectral signature does not take into account any bidirectional effect for the reflection on the Earth's surface. The model assumes a lambertian reflection on the surfaces. Due to this limitation, the modeling of spectral dependency of the reflected solar radiation is studied on flux instead of radiance:

$$F_{sol}^{uf} = F_{sol}^{uf}(\{F_{ch}\}) \tag{15}$$

and it is assumed that, dividing each flux F of 15 by π, the law will stay optimal for the unfiltered solar reflected radiance estimation.

6.2   Meteosat-7 case

6.2.1   Introduction

The main characteristics of the imager on-board Meteosat-7 are given in 3.4.2. This imager has only one channel in the solar reflected part of the spectrum : the visible channel (radiance noted as L_{vis}). The figure 7 shows the spectral response curve of this channel and the spectral response curves of the 3 SEVIRI solar reflected channels. The Meteosat-7 visible channel is sensitive to a great part of the reflected solar energy (more than 50% for most of the scene).

$$\frac{L_{vis}}{L_{vis}^{solspec}} = \frac{\int_0^\infty L(\lambda)\,\phi_{vis}(\lambda)\,d\lambda}{\int_0^\infty L^{solspec}(\lambda)\,\phi_{vis}(\lambda)\,d\lambda} \geq 50\%$$

where L_{vis} is the measured NB radiance in the visible band and $L_{vis}^{solspec}$ is the incident solar radiance caught by the spectral filter $\phi_{vis}(\lambda)$.

With Meteosat-7, the problem 15 becomes to find the function :
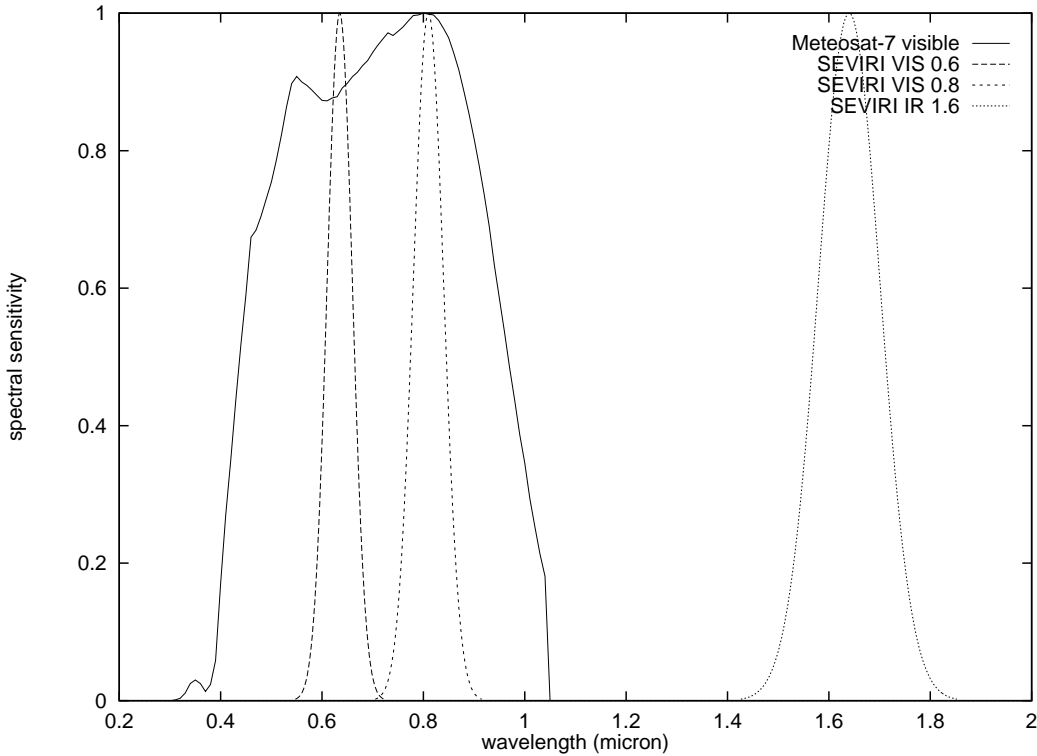
Figure 7: The curves of channels spectral response for the METEOSAT-7 visible band imager and for the 3 "solar reflected" SEVIRI channels.

$$F_{sol}^{uf} = F_{sol}^{uf}(F_{vis})$$

The figure 8 shows the distribution of (F_{vis}^{uf}, F_{vis}) for our data set of 2000 Earth-atmosphere scenes (see section §4.2).

6.2.2 Unfiltering using Radiances

With a polynomial expansion up to the third order on the visible band flux F_{vis}, the discarding of variables technique (see section §4.5) gives the results summarized in table 10. The input measured flux was contaminated with a $\eta = 5\%$ standard deviation Gaussian noise.

The table 10 shows that the second and third order terms do not improve significantly the unfiltering process. For the sake of robustness and simplicity, a first order law must be used :

#coef	law	ϵ_r (%)
1	$F_{sol}^{uf} = 1.63\,F_{vis}$	6.83
2	$F_{sol}^{uf} = 25.06 + 1.57\,F_{vis}$	6.15
3	$F_{sol}^{uf} = 20.76 + 1.61\,F_{vis} - 65\,10^{-6}\,F_{vis}^2$	6.12
4	$F_{sol}^{uf} = 20.1 + 1.62\,F_{vis} - 107\,10^{-6}\,F_{vis}^2 + 45\,10^{-9}\,F_{vis}^3$	6.12

Table 10: Laws for unfiltered solar reflected radiance F_{sol}^{uf} estimate from the visible channel of Meteosat-7 F_{vis}. The regressions are computed without taking into account the solar zenith angle θ_s and then the intensity of the illumination. A sensor noise of $\eta = 5\%$ is assumed for the imager channel.

Figure 8: Distribution of the unfiltered broadband solar reflected flux F_{sol}^{uf} (vertical axis) and Meteosat-7 visible band flux F_{vis} (horizontal axis) for the data set of 2000 random Earth-atmosphere scenes. Fluxes are expressed in Wm^{-2}.
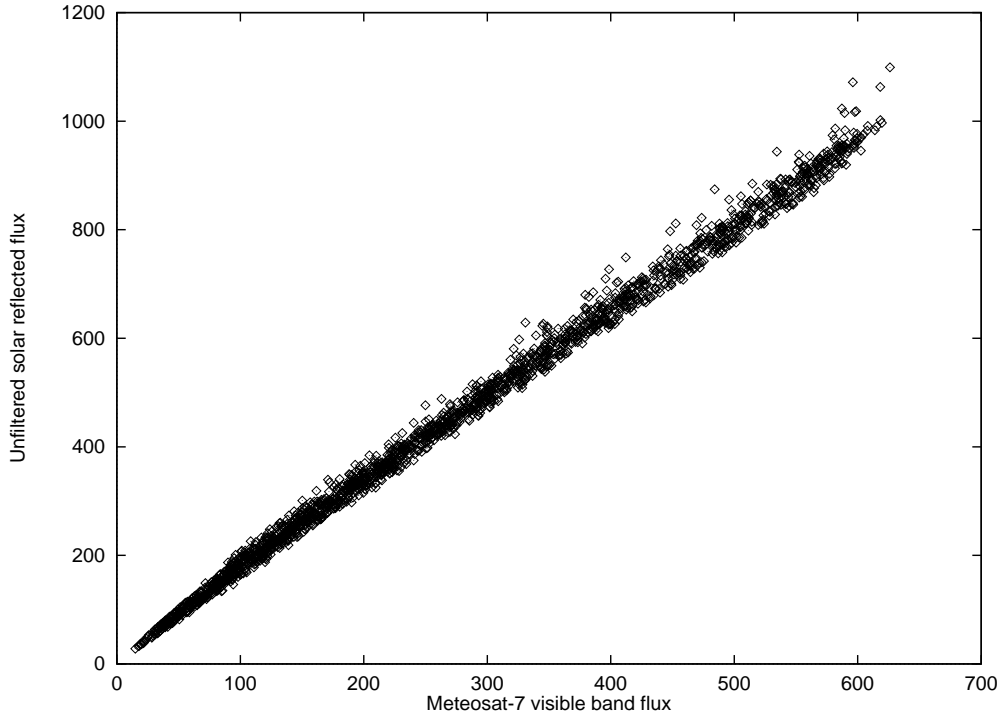
$$F_{sol}^{uf} = 25.06 + 1.57\,F_{vis} \tag{16}$$

6.2.3 Solar Zenith Angle θ_s Dependency

The table 11 gives the best first order regression for given solar zenith angles θ_s in the set $\{0^o, 10^o, 20^o, 30^o, 40^o, 50^o, 60^o, 70^o, 80^o\}$[3]. Doing this, one hopes to improve the performance of a hypothetic implicit scene identification process. With all solar zenith angles together, the scene dependence on the measured flux F_{vis} is masked by the high dependency of F_{sol} on the solar zenith angle.

One can see that there is not real improvement of the unfiltering process when the regression is computed at given solar zenith angles. The improvement can be estimated as a reduction of residual error from $\epsilon_r = 6.31\%$ to $\epsilon_r = 5.76\%$.

6.2.4 Dependence on the visible band imager noise

The residual error associated with the BB estimation formula 16 is strongly dependent on the imager noise η as shows the curve 9 and the results in table 12. For large error on F_{vis} (which is always the case for a weather satellite due to the absence of on-board calibration for solar channel(s)), the error on the estimated flux equals roughly the error on the sensor. On the other hand, even with a perfect sensor ($\eta = 0\%$), an asymptotic residual error of about $\epsilon_r = 4\%$ is inherent to the BB estimation with formula 16.

---

[3]For this study, 9 datasets was build usinmg SBDART with solar zenith angles of 0, 10, ..., 80 degrees. These dataset are stored in /planet/nic/RadiaTrans/Curves50degrees. For each of these solar zenith angles, 1000 curves are built with cloud cover and under clear sky conditions.

solar zenith angle θ_s	best first order regression	ϵ_r (%)
0°	$F_{sol}^{uf} = 46.86 + 1.524\,F_{vis}$	5.53%
10°	$F_{sol}^{uf} = 44.55 + 1.531\,F_{vis}$	5.74%
20°	$F_{sol}^{uf} = 43.03 + 1.532\,F_{vis}$	5.58%
30°	$F_{sol}^{uf} = 47.77 + 1.516\,F_{vis}$	5.80%
40°	$F_{sol}^{uf} = 38.20 + 1.539\,F_{vis}$	5.79%
50°	$F_{sol}^{uf} = 36.72 + 1.532\,F_{vis}$	5.72%
60°	$F_{sol}^{uf} = 26.10 + 1.562\,F_{vis}$	5.66%
70°	$F_{sol}^{uf} = 19.22 + 1.587\,F_{vis}$	5.84%
80°	$F_{sol}^{uf} = 9.877 + 1.627\,F_{vis}$	6.16%
all data together	$F_{sol}^{uf} = 26.468 + 1.564\,F_{vis}$	6.31%

Table 11: Best first order estimate of the BB radiance from the visible channels of Meteosat-7 at various viewing zenith angles θ_s and comparison when all data are merged together. A sensor noise of $\eta = 5\%$ is assumed for the imager channel.

noise level η on F_{vis}	residual error ϵ_r on F_{sol}^{uf}
0%	3.999 %
1%	4.123%
2%	4.452%
3%	4.945%
4%	5.557%
5%	6.255%
6%	7.012%
7%	7.811%
8%	8.642%
9%	9.494%
10%	10.364%

Table 12: Relative residual error ϵ_r on the unfiltered solar reflected flux estimated (using 16) from the single visible flux of Meteosat-7 with respect to the noise level η on this channel.
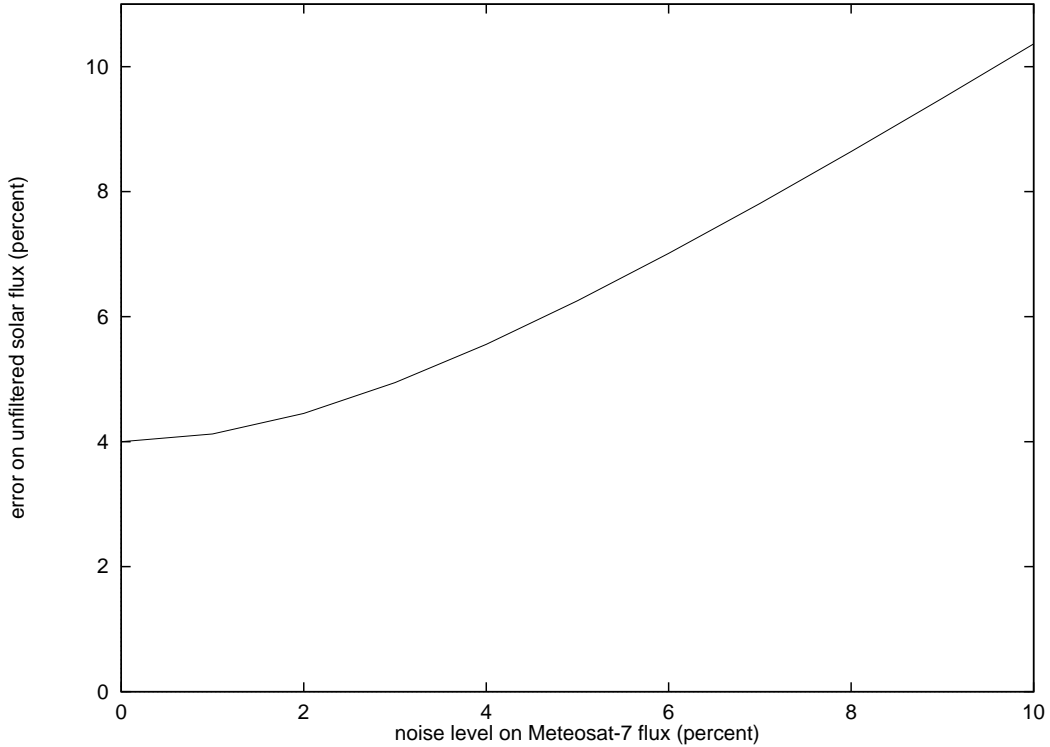
Figure 9: Relative residual error ϵ_r on the unfiltered solar reflected flux estimated (using 16) from the single visible flux of Meteosat-7 with respect to the noise level η on this channel.

6.2.5 Discussion

In the solar reflected region, the unfiltering with a single imager channel of type "visible" is always characterized with an important error ϵ_r: at least the error η on the measured imager radiance. In fact, when only one channel is available, the error can not be reduced by "noise averaging" on multiple channels.

With the imager of Meteosat-7, the possibility of implicit scene identification is weak, even when regressions are computed for a given solar zenith angles θ_s.

To allow a better implicit scene identification, one can :

1. use a multi-spectral imager as SEVIRI, this is studied in section §6.3,

2. use information from an external scene identification process ("explicit scene identification"),

3. use the clear sky radiance as additional information. Implicit comparison between the measured radiance and the clear sky radiance, may probably be helpful in the detection of cloud coverage. This study must be done in the future (TBD).

6.3 The SEVIRI case

6.3.1 Introduction

The main characteristics of SEVIRI are given in §3.4.3. As the HRV and the $IR_{3.8\mu}$ will not be used, 3 channels remain in the solar reflected part of the spectrum. The figure 7 shows the

#coef	law	ϵ_r (%)
1	$F_{sol}^{uf} = 12.89\,F_{0.8\mu}$	9.46
2	$F_{sol}^{uf} = 4.70\,F_{0.6\mu}\,+\,7.47\,F_{0.8\mu}$	5.62
3	$F_{sol}^{uf} = 24.28\,+\,5.10\,F_{0.6\mu}\,+\,6.48\,F_{0.8\mu}$	5.18
4	$F_{sol}^{uf} = 23.84\,+\,5.42\,F_{0.6\mu}\,+\,5.97\,F_{0.8\mu}\,+\,0.15\,F_{1.6\mu}^2$	4.77
4 bis	$F_{sol}^{uf} = 17.74\,+\,5.46\,F_{0.6\mu}\,+\,5.91\,F_{0.8\mu}\,+\,2.40\,F_{1.6\mu}$	4.89
	...	
10	all coefficients up to the second order...	4.60
	...	
20	all coefficients up to the third order...	4.46
	...	
35	all coefficients up to the fourth order...	4.40
	...	

Table 13: Best laws for unfiltered solar reflected flux F_{sol}^{uf} estimation when an increasing number of regression coefficients are used. Inputs are the $F_{0.6\mu}$, $F_{0.8\mu}$ and $F_{1.6\mu}$ SEVIRI fluxes. Each channel is contaminated with a $\eta = 5\%$ noise level.

spectral response curves of these channels and the table 2 gives the expected characteristics of these channels.

With SEVIRI, the unfiltered radiance inference from NB radiances consists in finding the function:

$$L_{sol}^{uf} = L_{sol}^{uf}(L_{0.6\mu}, L_{0.8\mu}, L_{1.6\mu})$$

Due to the limitations of the used radiative transfer model explained previously in section §6.1, fluxes are used instead of radiances:

$$F_{sol}^{uf} = F_{sol}^{uf}(F_{0.6\mu}, F_{0.8\mu}, F_{1.6\mu})$$

6.3.2 Results

Using the discarding of variables technique explained in section §4.5, the best regression laws are computed when an increasing number of coefficients are used. The table 13 summarizes these results when the input fluxes are all contaminated with a $\eta = 5\%$ Gaussian noise.

6.3.3 Discussion

1. The use of both the 0.6μ and 0.8μ channels is needed to get about the same accuracy than using the visible channel of Meteosat-7. This is due to the sharper shapes of the SEVIRI channels (see figure 7).

2. The residual error ϵ_r of the regression is under 5% for the solar reflected radiation. This is under the noise level $\eta = 5\%$ added to the inputs but is also about 5 times worse than for the estimate of the thermal unfiltered radiances.

3. The best use of the 1.6μ channel in the regression appears to be at the second power:

$$F_{sol}^{uf} = 23.84\,+\,5.42\,F_{0.6\mu}\,+\,5.97\,F_{0.8\mu}\,+\,0.15\,F_{1.6\mu}^2$$

Nevertheless, the first order law will be used in the following as the "reference law" :

$$F_{sol}^{uf} = 17.74\,+\,5.46\,F_{0.6\mu}\,+\,5.91\,F_{0.8\mu}\,+\,2.40\,F_{1.6\mu}$$

6.3.4   Loss of channel(s)

Here, we shortly analyze the implications of the loss of 1 of the 3 SEVIRI channels. For this, we use the second order regression :

$$F_{sol}^{uf} = \beta_0 + \beta_1 F_{0.6\mu} + \beta_2 F_{0.8\mu} + \beta_3 F_{1.6\mu} + \beta_4 F_{0.6\mu}^2 + \beta_5 F_{0.6\mu} F_{0.8\mu} +$$

$$\beta_6 F_{0.8\mu}^2 + \beta_7 F_{0.6\mu} F_{1.6\mu} + \beta_8 F_{0.8\mu} F_{1.6\mu} + \beta_9 F_{1.6\mu}^2 \tag{17}$$

input	ϵ_r (%)
all except $F_{0.6\mu}$	8.96
all except $F_{0.8\mu}$	7.77
all except $F_{1.6\mu}$	5.07
all inputs	4.60

Two of the 3 solar reflected SEVIRI channels appear to be "critical" for the accuracy of the inference process from the imager : the channel at 0.6μ and the channel at 0.8μ. The loss of one of these roughly double the error ϵ_r of the inference process! On the other hand, the loss (or the choice not to use) the channel at 1.6μ should not have great influence on the inference. If, simultaneously, the 0.6μ and 0.8μ channels are not available, the estimate of the unfiltered radiance is clearly impossible:

inputs	ϵ_r (%)
all except $L_{0.6\mu}$ and $L_{0.8\mu}$	55.68%

6.3.5   Solar zenith angle dependency

The residual error of the second order regression is given in table 14 when the regression is computed at given solar zenith angles in the set $\theta_s = \{0^o, 10^o, 20^o, 30^o, 40^o, 50^o, 60^o, 70^o, 80^o\}$. In this case, the averaged ϵ_r value is 4.45%. Compared with the $\epsilon_r = 4.6\%$ when solar zenith angle is not taken into account, one can say that there is no improvement of the unfiltering process when the regression is computed at given solar zenith angles.

6.3.6   Imager noise influence

The results given before were obtained using a typical $\eta = 5\%$ noise level on the imager measurements. Here, we will investigate the influence of this noise level on the unfiltering process accuracy.

The residual error ϵ_r associated with the unfiltering formula is strongly dependent on the imager noise η as shows the curve 10 and the results in table 15. With a perfect imager (that means without noise and with perfect calibration), an asymptotic residual error of about

$$\epsilon_r \rightarrow 3\%$$

is inherent to BB estimation process. For large error η on the imager measurements (this is always the case for weather satellite due to the absence of on-board calibration for solar channels), the error on the estimated broadband flux can be estimated by:

solar zenith angle	ϵ_r (%)
0°	4.213
10°	4.181
20°	4.224
30°	4.344
40°	4.380
50°	4.663
60°	4.539
70°	4.720
80°	4.821
all data together	4.682

Table 14: Residual error ϵ_r of the best second order regression to estimate the unfiltered solar reflected flux F_{sol}^{uf} from the 3 visible channels of SEVIRI when the regression is computed at given solar zenith angles θ_s. A sensor noise of $\eta = 5\%$ is assumed for the imager channels.

η (%)	ϵ_r (%)
0	2.976
1	3.053
2	3.289
3	3.648
4	4.094
5	4.597
6	5.138
7	5.704
8	6.288
9	6.884
10	7.488

Table 15: Relative residual error ϵ_r of the unfiltered solar reflected flux inference from the SEVIRI NB measurements with respect to the noise level on the imager measurements η. The second order regression 17 is used to build this table.

$$\epsilon_r \rightarrow \frac{\eta}{\sqrt{N}}$$

where η is the imagers noise level (assumed here to be the same for each channel) and N is the number of channels.

6.3.7 Discussion

In the solar reflected region, the unfiltered radiance estimation from the 3 NB SEVIRI channels is always characterized with an important error: $\epsilon_r > 3\%$. This error increases with the inevitable noise level η on the imager radiances. With a typical noise level of 5%, the F_{sol}^{uf} estimation is typically characterized with a $\epsilon_r = 4.5\%$ relative residual error. This is a bit better than using the single Meteosat-7 visible band channel ($\epsilon_r = 6.3\%$). Implicit scene identificationseems not be usefull in this BB estimation process.
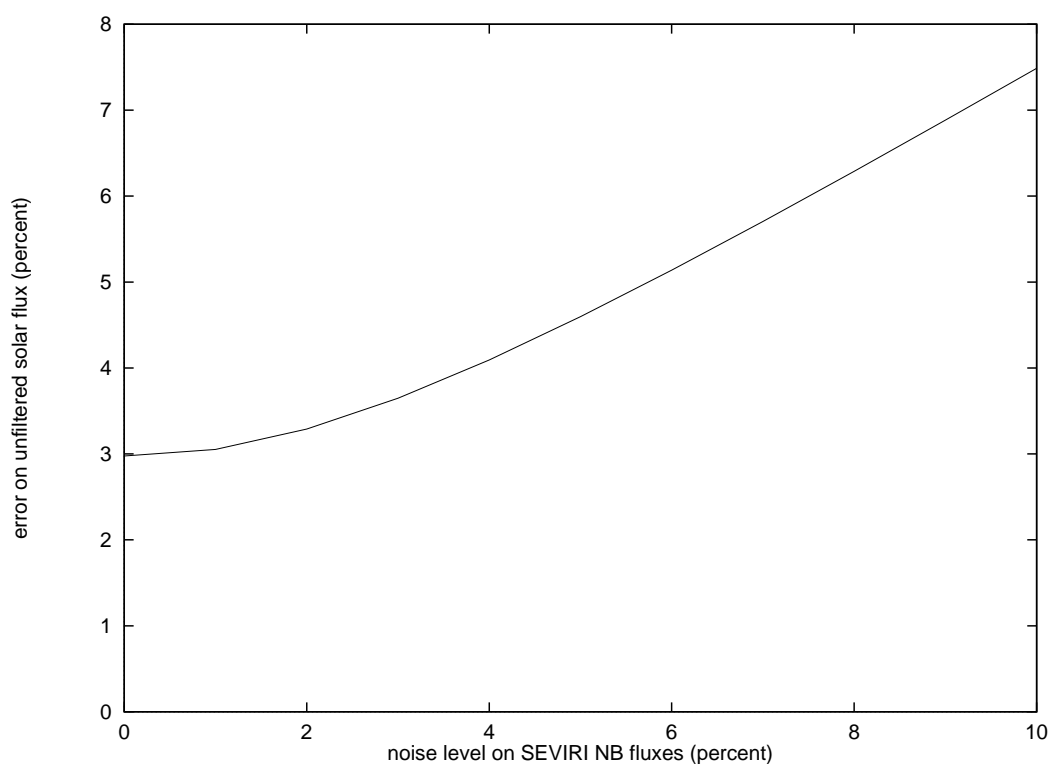
Figure 10: Relative residual error ϵ_r of the unfiltered solar reflected flux inference from the SEVIRI NB measurements with respect to the noise level on the imager measurements η. The second order regression 17 is used to build this figure.

6.4 Conclusions and discussion

Single law (first or second order regression) can (must) be used to infer the unfiltered radiance from NB radiance(s) of the imager in the solar reflected region. For Meteosat-7 and SEVIRI, the following regressions can be used :

$$F_{sol}^{uf} = 5.06 + 1.57\, F_{vis}$$

$$F_{sol}^{uf} = 17.74 + 5.46\, F_{0.6\mu} + 5.91\, F_{0.8\mu} + 2.40\, F_{1.6\mu}$$

1. Assuming a sensor noise level of $\eta = 5\%$, the residual errors for these regressions are respectively $\epsilon_r = 6.15\%$ and $\epsilon_r = 4.89\%$. This error is about 5 time worse than for the inference of unfiltered the thermal radiance.

2. The expected "implicit scene identification" does not appear in our results or appears in the form of a (very) weak improvement of the BB estimation process.

3. As for the thermal part of the spectrum, the noise level and error of calibration should be estimated carefully and should never be underestimated.

4. For the unfiltered solar reflected radiance estimation with an imager, the main advantage of SEVIRI with respect to Meteosat seems be that, by averaging the 0.6μ and 0.8μ channels, a reduction of the influence of the noise level (and calibration error) η is observed.

7 Broadband Radiometer Radiances Estimate Using Imager Data

7.1 Introduction

7.1.1 Quantities to be estimated

As said in 3.3, 4 filtered broadband quantities have to be estimated from the imager NB radiances: the short wave and long wave values of the solar reflected and thermal radiances:

solar reflected BB radiometer short wave radiance	$L_{sw,sol}^{filt} = \int_0^\infty L_{sol}(\lambda)\,\varphi_{sw}(\lambda)\,d\lambda$
thermal emission BB radiometer long wave radiance	$L_{lw,th}^{filt} = \int_0^\infty L_{th}(\lambda)\,\varphi_{lw}(\lambda)\,d\lambda$
solar reflected BB radiometer long wave radiance	$L_{lw,sol}^{filt} = \int_0^\infty L_{sol}(\lambda)\,\varphi_{lw}(\lambda)\,d\lambda$
thermal emission BB radiometer short wave radiance	$L_{sw,th}^{filt} = \int_0^\infty L_{th}(\lambda)\,\varphi_{sw}(\lambda)\,d\lambda$

The spectral response curves $\phi_{sw}(\lambda)$ and $\phi_{lw}(\lambda)$ of the GERB instrument were given in section §3.5.

7.1.2 Rough estimate of the filtered quantities

Typical curves for $F_{sol}(\lambda)$ and $F_{th}(\lambda)$ are computed using SBDART ("land" surface, solar zenith angle of 50 degrees, ...). Figure 11 shows these curves.

Using the CERES filters (see figures 2 and 3 from section §3.5), one gets the following filtered fluxes:

$$
\begin{aligned}
F_{sw,sol}^{filt} &= \int_0^\infty F_{sol}(\lambda)\,\varphi_{sw}(\lambda)\,d\lambda = 166.900\,Wm^{-2} \\
F_{lw,th}^{filt} &= \int_0^\infty F_{th}(\lambda)\,\varphi_{lw}(\lambda)\,d\lambda = 194.983\,Wm^{-2} \\
F_{lw,sol}^{filt} &= \int_0^\infty F_{sol}(\lambda)\,\varphi_{lw}(\lambda)\,d\lambda = -1.695\,Wm^{-2} \\
F_{sw,th}^{filt} &= \int_0^\infty F_{th}(\lambda)\,\varphi_{sw}(\lambda)\,d\lambda = 0.720\,Wm^{-2}
\end{aligned}
$$

These estimates of filtered fluxes have to be divided by π to get estimates of the filtered radiances $L_{sw,sol}^{filt}$, $L_{lw,th}^{filt}$, $L_{lw,sol}^{filt}$ and $L_{sw,th}^{filt}$. One can see that the $L_{lw,sol}^{filt}$ and the $L_{sw,th}^{filt}$ are very small with respect to $L_{sw,sol}^{filt}$ and $L_{lw,th}^{filt}$.

7.2 Thermally emitted Long wave Radiance

7.2.1 Statement

As the (synthetic) long wave filter is close to the flat filter in the thermal region, the inference of $L_{lw,th}^{filt}$ from the NB channel(s) of an imager should be very similar to the inference of L_{th}^{uf} that has been studied in detail in section §5. In particular, it has been proved that the dependency in viewing zenith angle θ_v must be take into account to reach best performances (see §5.5).

7.2.2 Meteosat-7 case

In view of the results obtained in §5.2, a first order regression is used to estimate $L_{lw,th}^{filt}$ from the water vapor L_{wv} and window L_{ir} radiances:
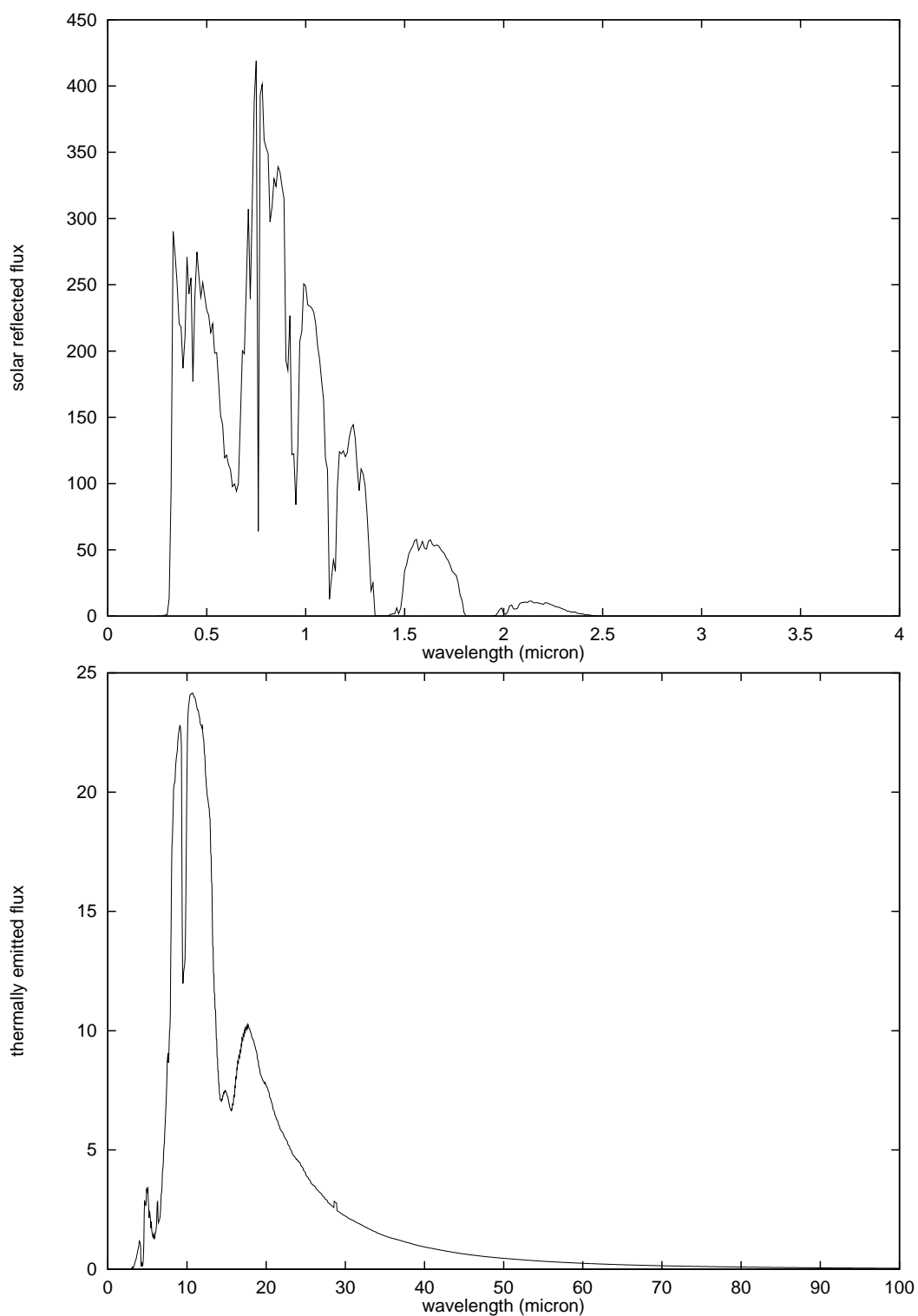
Figure 11: Typical solar reflected (top) and thermally emitted (bottom) spectral fluxes $(Wm^{-2}\mu^{-1})$ that are used to give a rough estimate of the filtered broadband radiometer radiances.

θ_v (degrees)	β_0	β_1	β_2	$\epsilon_{r\,(\%)}$
0	16.297	13.673	2.790	1.7948
10	16.300	13.707	2.785	1.7942
20	16.292	13.841	2.771	1.7945
30	16.284	14.058	2.748	1.7945
40	16.267	14.399	2.713	1.7986
50	16.230	14.912	2.663	1.8058
60	16.154	15.694	2.595	1.8229
70	15.979	16.953	2.503	1.8509
80	15.534	19.248	2.381	1.9007

Table 16: Best first order regression law for the estimate of $L_{lw,th}^{filt}$ from the Meteosat-7 thermal radiances L_{wv} (water vapor) and L_{ir} (window). $\{\beta_i\}$ are the coefficients of the regression 18.The relative residual error ϵ_r is relatively independent on the satellite viewing angle θ_v. A sensor noise of $\eta = 2\%$ is assumed for the imager channels.

$$L_{lw,th}^{filt} = \beta_0 + \beta_1 L_{wv} + \beta_2 L_{ir} \tag{18}$$

The regression coefficients β_i and associated residual errors ϵ_r are given in table 16 for various viewing zenith angles θ_v. The relative residual errors ϵ_r in table 16 are very similar to the residual error on the estimate of L_{th}^{uf} (see table 7).

7.2.3 SEVIRI case

In view of the results obtained in §5.3, a first order regression is used to estimate $L_{lw,th}^{filt}$ from the 7 SEVIRI thermal radiances :

$$L_{lw,th}^{filt} = \beta_0 + \beta_{6.2\mu}L_{6.2\mu} + \beta_{7.3\mu}L_{7.3\mu} + \beta_{8.7\mu}L_{8.7\mu} + \beta_{9.7\mu}L_{9.7\mu} + \tag{19}$$

$$\beta_{10.8\mu}L_{10.8\mu} + \beta_{12\mu}L_{12\mu} + \beta_{13.4\mu}L_{13.4\mu} \tag{20}$$

The regression coefficients $\{\beta_i\}$ and the associated residual errors ϵ_r are given in table 17 for various viewing zenith angles θ_v. The relative residual errors ϵ_r in table 17 are very similar to the residual error on the estimate of L_{th}^{uf} (see table 8).

7.3 Solar Reflected Short wave Radiance

7.3.1 Statement

As the short wave filter of the BB radiometer is close to the flat filter in the solar reflected region, the inference of $L_{sw,sol}^{filt}$ from the NB channel(s) of an imager should be very similar to the inference of L_{sol}^{uf} that has been studied in detail in section §6. In particular, it has been proved that the dependency in solar zenith angle θ_s may improve the weakly inferring process (see §11 and §6.3.5).

θ_v	ϵ_r (%)	β_0	$\beta_{6.2\mu}$	$\beta_{7.3\mu}$	$\beta_{8.7\mu}$	$\beta_{9.7\mu}$	$\beta_{10.8\mu}$	$\beta_{12\mu}$	$\beta_{13.4\mu}$
0°	1.0583	13.444	7.487	2.605	2.062	-0.492	1.039	1.027	4.053
10°	1.0583	13.428	7.497	2.596	2.069	-0.484	1.035	1.024	4.065
20°	1.0590	13.379	7.582	2.575	2.093	-0.480	1.024	1.016	4.087
30°	1.0564	13.290	7.678	2.551	2.124	-0.463	1.009	0.997	4.136
40°	1.0527	13.154	7.812	2.542	2.153	-0.435	0.988	0.979	4.199
50°	1.0446	12.955	7.960	2.589	2.166	-0.388	0.958	0.972	4.274
60°	1.0293	12.672	8.062	2.794	2.134	-0.314	0.920	0.988	4.349
70°	1.0022	12.285	7.939	3.454	1.965	-0.178	0.892	1.068	4.360
80°	0.9930	11.745	6.733	5.771	1.441	0.109	0.919	1.292	4.124

Table 17: Best first order regression law for the estimate of $L_{lw,th}^{filt}$ from the SEVIRI NB radiances $\{L_{ch}\}$. $\{\beta_{ch}\}$ and β_0 are the coefficients of the regression 20. The relative residual error ϵ_r is relatively independent on the satellite viewing angle θ_v. A sensor noise of $\eta = 2\%$ is assumed for the imager channels.

θ_s	β_0	β_1	ϵ_r (%)
0°	34.182	1.176	5.7044
10°	32.369	1.182	5.9132
20°	30.722	1.184	5.7716
30°	34.647	1.171	5.9807
40°	26.911	1.192	5.9781
50°	25.494	1.188	5.8953
60°	17.152	1.215	5.8536
70°	12.300	1.238	6.0629
80°	5.672	1.269	6.4418

Table 18: Best first order regression laws for the estimate of $L_{sw,sol}^{filt}$ from the Meteosat-7 visible band radiances F_{vis}. $\{\beta_i\}$ are the coefficients of the regression 22.The relative residual error ϵ_r is relatively independent on the solar zenith angle θ_s. A sensor noise of $\eta = 5\%$ is assumed for the imager channel.

7.3.2   Meteosat-7 case

In view of the results obtained in §6.2, a first order regression is used to estimate $L_{sw,sol}^{filt}$ from the visible band of the Meteosat-7 imager :

$$L_{sw,sol}^{filt} = \beta_0(\theta_s) + \beta_1(\theta_s)\, L_{vis} \tag{21}$$

As the flux is used instead of radiance, the regression becomes :

$$F_{sw,sol}^{filt} = \beta_0(\theta_s) + \beta_1(\theta_s)\, F_{vis} \tag{22}$$

The regression coefficients $\beta_i(\theta_s)$ and the associated residual errors ϵ_r are given in table 18 for various solar zenith angles θ_s. The relative residual errors ϵ_r in table 18 are very similar to the residual error of the estimate of L_{sol}^{uf} (see table 11).

7.3.3   SEVIRI case

In view of the results obtained in §, a first order regression is used to estimate $F_{sw,sol}^{filt}$ from the 3 SEVIRI solar reflected fluxes:

θ_s	ϵ_r (%)	β_0	$\beta_{0.6\mu}$	$\beta_{0.8\mu}$	$\beta_{1.6\mu}$
0°	4.6404	16.873	4.265	4.407	1.833
10°	4.6402	24.026	4.188	4.491	0.830
20°	4.5523	16.537	4.422	4.221	2.001
30°	4.6068	16.002	4.365	4.336	1.751
40°	4.7293	13.468	4.225	4.471	2.370
50°	4.8567	12.821	4.181	4.627	1.853
60°	5.0854	11.652	4.032	4.928	1.195
70°	5.1599	9.098	4.002	4.996	1.731
80°	5.2724	6.273	3.888	5.236	1.412

Table 19: Best first order regression law for the estimate of $F_{sw,sol}^{filt}$ from the SEVIRI NB fluxes $\{F_{0.6\mu}, F_{0.8\mu}, F_{1.6\mu}\}$. $\{\beta_{ch}\}$ are the weighting coefficients and β_0 the independent term. The relative residual error ϵ_r is relatively independent on the solar zenith angle θ_s. A sensor noise of $\eta = 5\%$ is assumed for the imager channels.

#coef	law	ϵ_r (%)
1	$F_{lw,sol}^{filt} = -0.01598\, F_{vis}$	7.21
2	$F_{lw,sol}^{filt} = -0.164 - 0.01555\, F_{vis}$	7.13
3	$F_{lw,sol}^{filt} = -0.291 - 0.01436\, F_{vis} - 1.93\,10^{-6}\, F_{vis}^2$	7.01
4	$F_{lw,sol}^{filt} = -0.612 - 0.0091\, F_{vis} - 22.4\,10^{-6}\, F_{vis}^2 + 21.9\,10^{-9}\, F_{vis}^3$	6.83

Table 20: Laws for the estimation of the solar reflected energy caught by the radiometer long wave filter $F_{lw,sol}^{filt}$ using as input information the Meteosat-7 visible band flux F_{vis}. A sensor noise of $\eta = 5\%$ is assumed for the imager channel.

$$F_{sw,sol}^{filt} = \beta_0(\theta_s) + \beta_{0.6\mu}(\theta_s)\, F_{0.6\mu} + \beta_{0.8\mu}(\theta_s)\, F_{0.8\mu} + \beta_{1.6\mu}(\theta_s)\, F_{1.6\mu} \qquad (23)$$

The regression coefficients $\beta_i(\theta_s)$ and the associated residual errors ϵ_r are given in table 19 for various solar zenith angles θ_s. The relative residual errors in table 19 are very similar to the residual error of the estimate of L_{sol}^{uf} (see table 14).

7.4 Solar Reflected Long wave Radiance

7.4.1 Statement

In this chapter, we study how to estimate the part of the solar reflected radiation that is caught by the long wave filter $\phi_{lw}(\lambda)$ of the broadband radiometer. Figure 12 shows the CERES synthetic long wave filter in the solar reflected region.

As $\phi_{lw}(\lambda)$ is small and negative in the solar part of the electro-magnetic spectrum, $L_{lw,sol}^{filt}$ is expected to be small and negative. The inference of $L_{lw,sol}^{filt}$ from the solar reflected NB channel(s) is studied in this section. The dependency on the solar zenith angle θ_s is supposed negligible here.

7.4.2 Meteosat-7 case

The discarding of variables technique is applied to the problem of inferring $F_{lw,sol}^{filt}$ from the visible band flux F_{vis} of Meteosat-7. Results are summarized in table 20.

For the sake of robustness and simplicity, the table 20 shows that a first order law must be used :
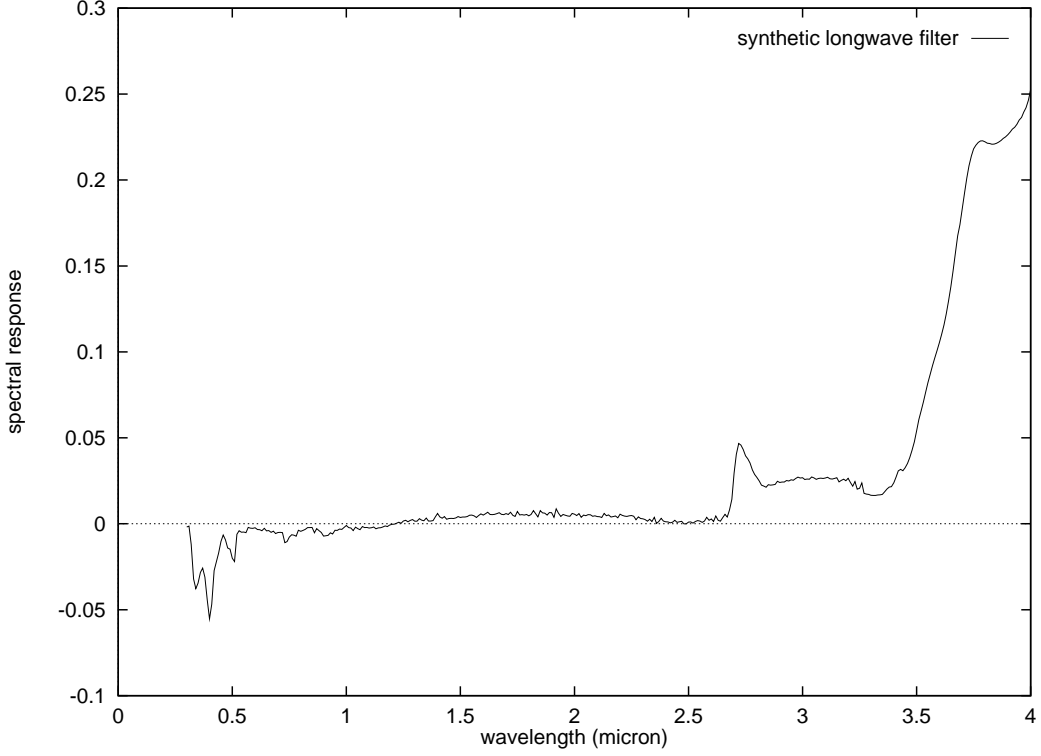
37

Figure 12: CERES synthetic long wave filter $\phi_{lw}(\lambda)$ in the solar reflected region. The negative spectral responses are due to the definition of the synthetic filter by equation 1.

$$F_{lw,sol}^{filt} = -0.01598\, F_{vis}$$

This estimation is subject to a error $\epsilon_r = 7.21\%$ when the input flux is submitted to a noise level of $\eta = 5\%$. Note that without error on the input flux ($\eta = 0\%$) the inference error falls to $\epsilon_r = 5.3\%$.

7.4.3 SEVIRI case

The discarding of variables technique is applied to the problem of inferring $F_{lw,sol}^{filt}$ from the 3 solar reflected NB fluxes of SEVIRI $\{F_{0.6\mu}, F_{0.8\mu}, F_{1.6\mu}\}$. Results are summarized in table 21.

In the table 21, the 0.6μ and 0.8μ channels appear with negative weighting in the regression but the 1.6μ channel appears with positive weighting. This is explained by the sign of the long wave filter $\phi_{lw}(\lambda)$ at these wavelengths.

#coef	law	$\epsilon_r\,(\%)$
1	$F_{lw,sol}^{filt} = -0.108\, F_{0.6\mu}$	8.54
2	$F_{lw,sol}^{filt} = -0.073\, F_{0.6\mu} - 0.041\, F_{0.8\mu}$	6.52
3	$F_{lw,sol}^{filt} = -0.3177 - 0.079\, F_{0.6\mu} - 0.028\, F_{0.8\mu}$	5.70
4	$F_{lw,sol}^{filt} = -0.3914 - 0.074\, F_{0.6\mu} - 0.034\, F_{0.8\mu} + 0.027\, F_{1.6\mu}$	5.44

Table 21: Laws for the estimation of the solar reflected energy caught by the radiometer long wave filter $F_{lw,sol}^{filt}$ using as input information the SEVIRI NB fluxes. A sensor noise of $\eta = 5\%$ is assumed for the imager channel.
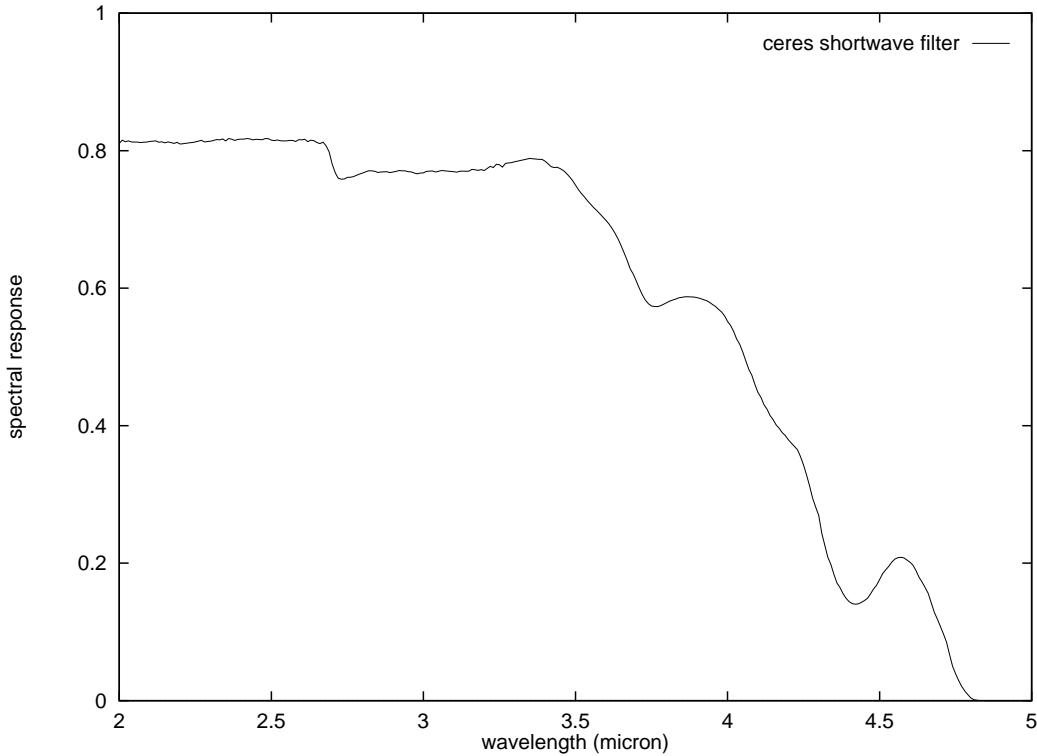
Figure 13: CERES short wave filter $\phi_{sw}(\lambda)$ in the cut-off region between 2μ and 5μ.

For the sake of robustness and simplicity, the table 21 shows that a first order law must be used :

$$F_{lw,sol}^{filt} = -0.3177 - 0.079\,F_{0.6\mu} - 0.028\,F_{0.8\mu}$$

This estimation is subject to a $\epsilon_r = 5.7\%$ error when the input flux is submitted to a noise level of $\eta = 5\%$. Note that without error on the input fluxes ($\eta = 0\%$) the inference error falls to $\epsilon_r = 3.8\%$.

7.5 Thermally emitted Short wave Radiance

7.5.1 Statement

In this chapter, we study how to estimate the part of the Earth's thermal emission that is caught by the short wave filter $\phi_{sw}(\lambda)$ of the broadband radiometer. Figure 13 shows the shape of the CERES short wave filter in the cut-off region. Figure 2 also shows that the quartz filter which is supposed to absorb all long wave radiation becomes semi-transparent for far infra-red radiation ($\lambda > 60\mu$).

Using the typical spectral curve $F_{th}(\lambda)$ given in figure 11, one can split the thermally emitted energy that is caught by the radiometer short wave filter $\phi_{sw}(\lambda)$ in two parts : the near-ir ($\lambda < 25\mu$) and the far-ir ($\lambda > 25\mu$).

$$F_{th}^{unfilt} = \int_0^\infty F_{th}(\lambda)\,d\lambda = 253.71\,Wm^{-2}$$
$$F_{sw,th}^{filt} = \int_0^\infty F_{th}(\lambda)\,\varphi_{sw}(\lambda)\,d\lambda = 0.720\,Wm^{-2}$$
$$F_{sw,th}^{filt,near-ir} = \int_0^{25\mu} F_{th}(\lambda)\,\varphi_{sw}(\lambda)\,d\lambda = 0.4687\,Wm^{-2}$$
$$F_{sw,th}^{filt,far-ir} = \int_{25\mu}^\infty F_{th}(\lambda)\,\varphi_{sw}(\lambda)\,d\lambda = 0.2513\,Wm^{-2}$$

#coef	law	ϵ_r (%)
1	$L_{sw,th}^{filt} = 0.0195\,L_{ir}$	24.52
2	$L_{sw,th}^{filt} = 0.1853 + 0.000389\,L_{ir}^2$	15.48
3	$L_{sw,th}^{filt} = 0.3669 - 0.01498\,L_{ir} + 0.000645\,L_{ir}^2$	13.23
4	$L_{sw,th}^{filt} = 0.3573 - 0.01368\,L_{ir} - 0.000312\,L_{wv}L_{ir} + 0.000642\,L_{ir}^2$	13.24
...	...	
6	all up to the second order	12.96
	...	
10	all up to the third order	12.96
	...	

Table 22: Laws for the estimation of the thermally emitted radiation caught by the radiometer short wave filter $L_{sw,th}^{filt}$ using as input information the Meteosat-7 thermal radiance L_{wv} and L_{ir}. A sensor noise of $\eta = 2\%$ is assumed for the imager channels.

As one can see, the $F_{sw,th}^{filt,far-ir}$ is not negligible respect to $F_{sw,th}^{filt,near-ir}$.

7.5.2   Meteosat-7 case

The discarding of variables technique is applied to the problem of inferring $L_{sw,th}^{filt}$ from the two thermal channels of Meteosat-7 : L_{wv} (water vapor) and L_{ir} (ir window). Results are summarized in table 22.

The table 22 indicates that the water vapor channel (near 6μ) is not an informative input to infer $L_{sw,th}^{filt}$.For the sake of robustness and simplicity, the table 22 shows that a second order law on L_{ir} only must be used :

$$L_{sw,th}^{filt} = 0.3669 - 0.01498\,L_{ir} + 0.000645\,L_{ir}^2$$

This estimation is subject to a residual error $\epsilon_r = 13.2\%$ when the input radiances of Meteosat-7 are submitted to a noise level of $\eta = 2\%$. Note that without error on the input fluxes ($\eta = 0\%$) the inference error falls to $\epsilon_r = 12.8\%$.

7.5.3   SEVIRI case

The discarding of variables technique is applied to the problem of inferring $L_{sw,th}^{filt}$ from the 7 thermal channels of SEVIRI (channel 3.8μ is not take into account due to the solar reflected influence during the day) . Results are summarized in table 22.

The table 23 indicates that the more informative input to infer $L_{sw,th}^{filt}$ is the $L_{8.7\mu}$ channel at the second order. In the sake of robustness and simplicity, the table 23 shows that a second order law on $L_{8.7\mu}$ only gives better results than the first order law on all the 7 narrow-band radiances :

$$L_{sw,th}^{filt} = 0.246 + 0.00613\,L_{8.7\mu}^2$$

This estimation is subject to a $\epsilon_r = 9.48\%$ error when the input radiances are submitted to a noise level of $\eta = 2\%$.

#coef	law	ϵ_r (%)
1	$L^{filt}_{sw,th} = 0.0869\, L_{8.7\mu}$	18.97
2	$L^{filt}_{sw,th} = 0.246 + 0.00613\, L^2_{8.7\mu}$	9.48
3	$L^{filt}_{sw,th} = 0.0498\, L_{13.4\mu} + 0.00953\, L^2_{8.7\mu} - 0.00231\, L_{12\mu}L_{13.4\mu}$	8.29
4	$L^{filt}_{sw,th} = 0.1656 + 0.0189\, L_{12\mu} + 0.0196\, L^2_{8.7\mu} - 0.00707\, L_{8.7}L_{12\mu}$	7.70
	...	
7	all up to the first order	10.33
	...	
36	all up to the second order	6.72
	...	

Table 23: Laws for ythe estimation of the thermally emitted radiation caught by the radiometer short wave filter $L^{filt}_{sw,th}$ using as input information the 7 SEVIRI NB thermal radiances. A sensor noise of $\eta = 2\%$ is assumed for these imager channels.

7.6 Conclusions and Discussions

1. The estimation of the 4 filtered radiances of the radiometer from the NB radiances of the imager on a weather satellite has been studied in the case of the Meteosat-7 imager and of SEVIRI.

2. The estimates of $L^{filt}_{sw,sol}$ and $L^{filt}_{lw,th}$ have shown to be close to the estimate of the unfiltered broadband radiances (respectively L^{uf}_{sol} and L^{uf}_{th}). The same regression laws are planned to be used but with adapted coefficients. The residual errors ϵ_r of these inferences have shown to be close to the ones of the inferences of the unfiltered radiances.

3. The estimates of $L^{filt}_{lw,sol}$ can be done with first order regression on the NB radiances and is subject to a $\epsilon_r \approx 6\%$ residual error.

4. The estimates of $L^{filt}_{sw,th}$ needs a higher order regression (second order) on the NB radiances and is subject to a $\epsilon_r \approx 7\%$ (SEVIRI) to $\epsilon_r \approx 13\%$ (Meteosat-7) error.

8 Implementation

A single RMIB program ('nb2bb') takes as inputs:

1. the viewing angles images θ_v, θ_s, ϕ (floating point images),

2. a parameters file that contains the coefficients of the various regressions studied in this document,

3. the imager NB radiances images for both solar reflected and thermal channels (floating point images),

and generates as output the 6 images of (unfiltered or filtered) broadband radiances as floating point images.

narrow-band radiances of the imager

viewing angles
images

regressions coefficients

...

nb2bb

filtered BB radiances

unfiltered radiances
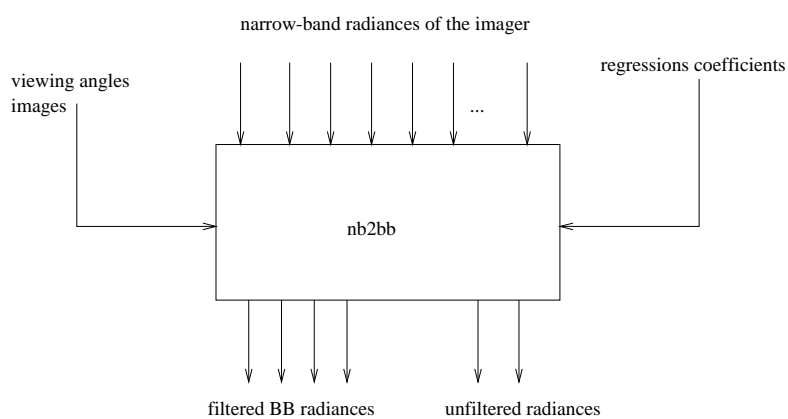
quantities	METEOSAT-7	SEVIRI	section
L_{th}^{uf}	1.7%	1.0%	§5
L_{sol}^{uf}	5.7%	4.5%	§6
$L_{lw,th}^{filt}$	1.8%	1.0%	§7.2
$L_{sw,sol}^{filt}$	5.8%	4.7%	§7.3
$L_{lw,sol}^{filt}$	7.2%	5.7%	§7.4
$L_{sw,th}^{filt}$	13.2%	9.5%	§7.5

Table 24: Relative residual errors ϵ_r that are introduced by the inference processes. Input radiances are supposed to have a noise level of $\eta = 2\%$ for the thermal channels and $\eta = 5\%$ for the solar reflected channels. The related section in this document are given in the last column.

9   Conclusions

1. This document summarizes various experiences that were done at RMIB in order to understand and improve the scene modeling which is an important step in the unfiltering of data generated by a BB radiometer using data provided by a (poorly calibrated) imaging device.

2. Emphasis was put on the couples of sensors: GERB/Meteosat-7 and GERB/SEVIRI. To date, the spectral response curves of CERES are used as representative of the GERB spectral response curves.

3. The table 24 summarizes the relative residual errors ϵ_r introduced on the 6 inferred radiances when input information for the spectral modeling are provided by the imager of METEOSAT-7 and by SEVIRI. In both cases, an error noise of $\eta = 5\%$ (shortwave) and $\eta = 2\%$ (thermal) were assumed for the radiances generated by the imager.

References

[NC01]   "Generation of a Data Set of Earth's Scenes Spectral Signature", RMIB GERB Ground
            Segment internal documentation, Nicolas Clerbaux, June 1999.

[SSP]   "SEVIRI Science Plan", Version1, 27 march 1998, EUMETSAT (available for down
            load from EUMETSAT web site, http://www.eumetsat.de/publication)

[PINT]   "The integral program', RMIB library documentation, 1999.

[MA79]   "Multivariate Analysis", K.V.Mardia, J.T.Kent and J.M.Bibby, 1979, Academic Press.

[PLMS]   "Least Square User's Manual", BATS library documentation, 1999.

[FILT]   "Spectral Response Curves used at RMIB for the GERB Ground Segment", GERB
            Ground Segment documentation, Nicolas Clerbaux 1999.

[SBDART] "Santa Barbara Disort Atmospheric Radiative Transfer : A Practical Tool for Plane-
            Parallel Radiative Transfer in the Earth's Atmosphere", P. Ricchiazzi, S. Yang and
            C. Gautier, Earth Space Research Group, Institute for Computational Earth Sys-
            tem Science, University of California, Santa Barbara. Available from web site :
            http://arm.mrcsb.com/sbdart.

[AD6]   "RGP: GERB Processing", L. Gonzalez and A. Hermans, RMIB documentation MSG-
            RMIB-GE-TN-0006, June 29th 1999.